REAL-TIME SURFACE CHARGE MEASUREMENT OF BIOLOGICAL CELL USING MICRO ELECTROPHORESIS AND COMPACT CHARGE-COUPLED DEVICE (CCD) MICROSCOPE

TEOH BOON YEW

MASTER OF ENGINEERING SCIENCE

LEE KONG CHIAN FACULTY OF ENGINEERING AND SCIENCE

UNIVERSITI TUNKU ABDUL RAHMAN

SEPTEMBER 2015

REAL-TIME SURFACE CHARGE MEASUREMENT OF BIOLOGICAL CELL USING MICRO ELECTROPHORESIS AND COMPACT CHARGE-COUPLED DEVICE (CCD) MICROSCOPE

By

TEOH BOON YEW

A dissertation submitted to the Institute of Postgraduate Studies and Research,
Lee Kong Chian Faculty of Engineering and Science,
Universiti Tunku Abdul Rahman,
in partial fulfilment of the requirements for the Master of Engineering Science
September 2015

DECLARATION

I hereby declare that this project report is based on my original work except for citations and quotations which have been duly acknowledged. I also declare that it has not been previously and concurrently submitted for any other degree or award at UTAR or other institutions.

Signature : _____

Name : Teoh Boon Yew

ID No. : 12UEM07920

Date : / 9 /2015

APPROVAL SHEET

This dissertation entitled "***REAL-TIME SURFACE CHARGE MEASUREMENT OF BIOLOGICAL CELL USING MICRO ELECTROPHORESIS AND COMPACT CHARGE-COUPLED DEVICE (CCD) MICROSCOPE*****"** was prepared by **TEOH BOON YEW** and submitted as partial fulfillment of the requirements for the Master of Engineering science at Universiti Tunku Abdul Rahman.

Approved by:

_____

(Dr.Lee Poh Foong) Date:……..
Supervisor
Department of Mechatronics and BioMedical Engineering
Lee Kong Chian Faculty of Engineering and Science
Universiti Tunku Abdul Rahman

_____

(Dr. Yong Thian Khok) Date:……..
Co-supervisor
Department of Electrical and Electronic Engineering
Lee Kong Chian Faculty of Engineering and Science
Universiti Tunku Abdul Rahman

The copyright of this report belongs to the author under the terms of the copyright Act 1987 as qualified by Intellectual Property Policy of Universiti Tunku Abdul Rahman. Due acknowledgement shall always be made of the use of any material contained in, or derived from, this report.

© 2015, Teoh Boon Yew. All right reserved.

Specially dedicated to

my beloved fiancé, mother, father and family members.

ACKNOWLEDGEMENTS

I would like to thank everyone who had contributed to the successful completion of this project. I would like to express my gratitude to my research supervisor, Dr. Lee Poh Foong for her invaluable advice, guidance and her enormous patience throughout the development of the research.

In addition, I would also like to express my gratitude to my loving parent and friends who had helped and given me encouragement. Especially my fiancé, whose has given me physical support and emotional support.

ABSTRACT

REAL-TIME SURFACE CHARGE MEASUREMENT OF BIOLOGICAL CELL USING MICRO ELECTROPHORESIS AND COMPACT CHARGE-COUPLED DEVICE (CCD) MICROSCOPE

Teoh Boon Yew

Surface charge measurement of biological cells plays an important role in the study of cancer and malignant transformation. The existing methods for the surface charge measurement did not illustrate the physical information of the cell which being measured. These methods also inflicted long processing time and considered high processing cost per sample. The most common method used for the surface charge measurement is cell electrophoresis. In this study, micro electrophoresis method and compact CCD microscope with automated image processing was designed and built to measure the surface charge and display the physical information of the biological cells. The CCD microscope used magnification value of 125 X. With the Horn-Schunck image processing method, the images captured were processed automatically in real time to obtain the surface charge of the cell. The biological cells used in this study are yeast cell, normal bone cell (hFob 1.19), cancerous bone cell (U2OS), and cancerous cervical cell (HeLa). Polystyrene beads' (10μm ± 0.1μm) surface charge was measured using commercial instrument (ZETASIZER Melvan instrument) and compare with result obtained using compact CCD microscope system suggested in this study. The results measured by these two instruments showed 13% of variances. Yeast cells were selected control sample as biological single cells in this study. Results showed that the yeast cells were negatively charged in electrophoretic mobility throughout the pH range from 4 to 8. Aside from that, the negative electrophoretic mobility of yeast cells were increased proportionally with increased applied voltage. In this study, the normal bone cells and cancerous bone cells showed an exact match in volatile changing pattern of the electrophoretic mobility throughout the pH range, moreover, surface charge of cancer bone cells is higher in negativity than normal bone cells at pH 7 to pH 8 (pH value of Human blood). In addition, surface charge of HeLa cell was measured and found to have the

same surface charge trend compare to U2OS cell. In conclusion, the real time surface charge measurement set up for this study is able to measure the surface charge of biological cell. These results showed that the surface charge of normal cell and cancerous cells are difference in buffer solution range from pH 7 to pH 8.

TABLE OF CONTENTS

LIST OF FIGURES

LIST OF SYMBOLS / ABBREVIATIONS

E	electric field
ζ	surface potential
κ	Debye-Huckel
$\propto$	surface charge
v_{eo}	fluid velocity (electroosmosis)
v_{ep}	fluid velocity (electrophoretic)
μ_{ep}	electrophoretic mobility
ε	permittivity of the solution
η	Viscosity of the solution
α	Global smoothness

LIST OF APPENDICES

CHAPTER 1

INTRODUCTION

1.1 Application of surface charge

Study of surface charge has a broad range of technological applications in many industries including food production (Chaprenet et al., 2014), photographic emulsions (Howe, 2000), and pharmaceuticals (Karner and Anne, 2011). Study of surface charge is not only restricted to the different industries; it could be applied in the area of research to measure and to study cell to cell interaction. For instance, the study of ion transport activities was carried out by Latorre group in 1992. This study used the surface charge of the particle as a parameter to identify the transport activities on cell surface membrane. Other application of surface charge measurement includes the study of possible treatment for cancer disease such as the drug delivery process which liposome is used to deliver drug to target cells. Surface charge of liposome is measured in order to maintain colloid stability during drug delivery process (Allison, 2007). The study carried out by Zhang et al. (2011) showed that the surface charges of the cells (normal cells and cancer cells) change distinctively after being incubated with the coated nanoparticles. These studies showed that the negativity surface charge of the cancer cells reduce faster than the normal cell incubated with the nanoparticle. Hence the author suggested that the surface charge of the cell can be used as a parameter to indicate the effect of nanoparticle on living cell. In the study carried by Zhang and group, normal breast epithelia cell (MCF-10A) and cancerous breast cell (MCF-7) was used for the experiment together with surface charge measurement. These studies suggested that

quantitative measurement of biological particles' properties (such as the size and surface charge) is valuable, with regards to research and study of pharmaceutical applications.

Electrophoresis of cells was used as techniques to quantify surface charge and study the reaction at the level of membranes of the cell. This technique measures the cells which are suspended in an electrolytic medium and free to move in an electrified field. Since 1920, this method has been used by scientists to identify the motion of biological cell under an applied electric field (Coulter, 1920). Several methods had been developed, to determine the surface charge of particles under experimental conditions. The objective of these methods used was aimed at determining the surface charge of the cell as near to the natural surface charge property as possible. Measurement of biological particle's surface charge is routinely performed using phase analysis light scattering technique (PALS). This method estimates the electrophoretic mobility of the particles in an applied electric field by obtaining their average Brownian motion (Corbett et al., 2012). PALS present the average surface charge values of multiple particles. Therefore, accuracy in estimating surface charge particles depends on the mobility and size of particles, which can suffer errors that are made in average measurement, especially in complex population.

Numerous methods and techniques have been developed to measure the electrical properties of single particle, such as the coulter counter method (Dextras et al., 2009; Takahashi et al., 2011; Corbett et al., 2012). Coulter counter are able to measure the mobility of micron size particle, but the signal of the measurement is compromised in between signal to noise ratio of the surface charge measurement due to the different optimum orifice lengths (Takahashi et al., 2011).

The above mentioned methods (PALS) provide the surface charge value of the measured particle without any images of the particle during the measurement process. The physiological data of the measured particles is important for researchers to fully understand the effects of the measurement on the particles and the alternation of the particles during measurement. Furthermore, the process of the surface charge measurement using either the coulter counters or PALS is time consuming for a complex sample. For instance, coulter counter measures one particle at a time,

average surface charge of particles were calculated, this process requires long processing time. Long processing time always leads to biological cell death and nutrition depletion over time. Furthermore, cost per sample for surface charge measurement with these instruments is high. Measurement chamber of the mentioned methods are disposable where one chamber is only used for one sample at a time. Consequently, the measurement cost for one sample is high and only provide one time use only.

1.2 Surface charge of biological cell

Cells as the most basic component of every living organism has an enormous amount of extraordinary information packed within its intracellular organelles that contains codes for genetic product expressed on the cell surface membrane. Surface membrane of biological cells involved in an enormous type of interaction in between the cells and its environment; studies show (Dobrzyn and Figaszewski, 2013; An et al, 2009) that the cell membrane damages appear to display the status of disease and its status during treatment. Development of organism and its aspect for good health are maintained throughout life via the membranes of various types of cells. Highly specific reactions take place at the surface of cell involved in the chemical nature, composition and properties of cell. Tracing back to the origin of these reaction properties, (chemical, chemical-colloid and physical) all the reaction is electrochemically in nature.

A value of electric charge that is accumulated on the membrane of cell surface reflects the condition of the cell (Dobrzyn and Figaszewski, 2013). The increase of the membrane surface charge is often associated to malignancies of the cell (Dobrzyn and Figaszewski, 2013). In opposition, decrease of the surface charge is detected in dead cell. Transition of a cell from a healthy to pathological state causes alteration of the membrane surface charge, indicating study of the surface charge of cell has the potential for electrophysiological markers which can be used in the detection and diagnosis of disease. Study of membrane surface charge had acquired significance knowledge in the area of ion transport activities (Latorre, 1992),

cell to cell interaction (Van oss, 1994), cell macromolecule interaction (Simionescu, 1991) and motility of cell (Zhang et al., 2011; An et al., 2009; Gascoyne et al., 1994).

Therefore, surface charge measurement of biological cells serves a great potential in application of cancer research and other pharmaceutical application. However, these techniques (coulter counter and PALS) as mentioned in section 1.1 did not displayed a real time images of the particles or biological cell being measured. Furthermore, morphological or physical information of the cells were not shown while measurement is taking place. At the same time, long measuring time of these systems can cause the biological cell death due to depletion of medium. Cost per sample of these measurement techniques can be high, hence in this study, a real time, compact and cost effective surface charge measurement methods had been built.

1.3 Aims and Objectives

In this study, a comprehensive prototype has been developed, which utilizes image processing with electrophoresis system for surface charge measurement of biological cell. Morphology of the cell can be observed using imaging techniques in the micro electrophoresis system and surface charge of the cell is measured on real time basis. The image processing technique is commonly used in particle tracking and pattern recognition. Image processing techniques use two main approaches to track movement of migrating cell in a control environment: Firstly, cell segmentation and secondly cell association. By achieving both of the cell segmentation and association, the cells' projection and velocity is calculated. Acquiring the velocity information of the cell, the surface charge of the cell was calculated. The Smoluckski algorithm (Smoluchowski, 1917) is used for the measurement of the surface charge. The image processing method is suitable for acquiring the morphology information and measure the surface charge of cells at the same time. In this study, cancer cells' and normal cells' surface charge is measured and compared. Bone cancer cells and normal bone cells are selected as the cell line. At the same time, yeast cells and cervical cancer cells' surface charge are measured using the same control experiment condition. Polystyrene bead with the size of 10 μm is used to calibrate the

magnification of the compact CCD microscope. The pH value of the buffer solution is chosen as the controlled experiment condition.

The main objective of this study is to develop and build a compact CCD microelectrophoresis system with image processing for surface charge measurement. In order to achieve this objective, this work has been divided into three phases as follow:

- To develop and build a cost effective, compact CCD base microscope with microelectrophoresis system.
- To develop real time automated surface charge measurement system.
- To investigate the biological cell surface charge using CCD base microelectrophoresis with image processing method.

CHAPTER 2

LITERATURE REVIEW

2.1 Introduction

In this chapter, reviews of the surface charge measurement techniques, automated image processing techniques, theory of the cell surface charge measurement and various finding of studies related with biological cell's surface charge are discussed. The review of these studies help to conclude the methods used for our system and the optimum methods was chosen for this study.

2.2 Surface charge measurement

Several variations in methods (Coulter counter and PALS methods) have been developed to ensure and avoid artefacts in measurement of particle's surface charge. The methods include phase analysis light scattering which utilizes laser light scattering techniques, coulter counter, mass spectrometry, and suspended micro channel resonators. Detail of these methods will be discussed in the following section.

2.2.1 Phase analysis light scattering

Generally, the Electrophoretic mobility (EPM) of individual cells were determined by the conventional techniques of phase analysis light scattering (Corbett et al., 2012) method with cell electrophoresis. This method does not cause considerable damage

on viable cells. This method measures the average Brownian motion of the particles to estimate the average size and electrophoretic mobility of the overall multiple particles in an applied electric filed. The condition of the particles can be complex in population and multi-dimensional. The particles' condition in the measurement is assumed to disperse regularly throughout the whole measurement chamber.

Two electrodes were used in the measuring chamber while the sample placed in between these two electrodes (Figure 2.1). The two electrodes are supplied with electricity which induces the mobility. This method uses laser as the light source for screening through the samples and also piezo mirroring for comparison purposes. The mirror stands as a referring signal for the detector. The schematic diagram of the system built is shown in Figure 2.2. Even though it is applicable to a wide variety of particles, the result may suffer error from the average value of the calculation. This technique does not provide the physiological information of particles being measured. Results displayed are an average calculation of overall cells.

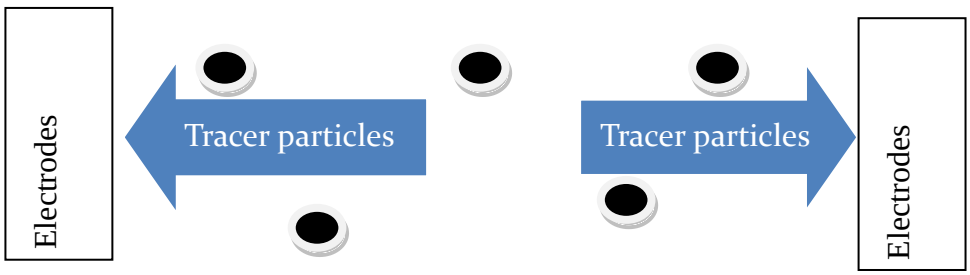

Figure 2.1: The measurement chamber set up for the phase analysis light scattering technique (Corbett et al., 2012). The electrophoretic mobility were measured as particles are place in the measurement chamber and applied electric field is supplied via a power supply.

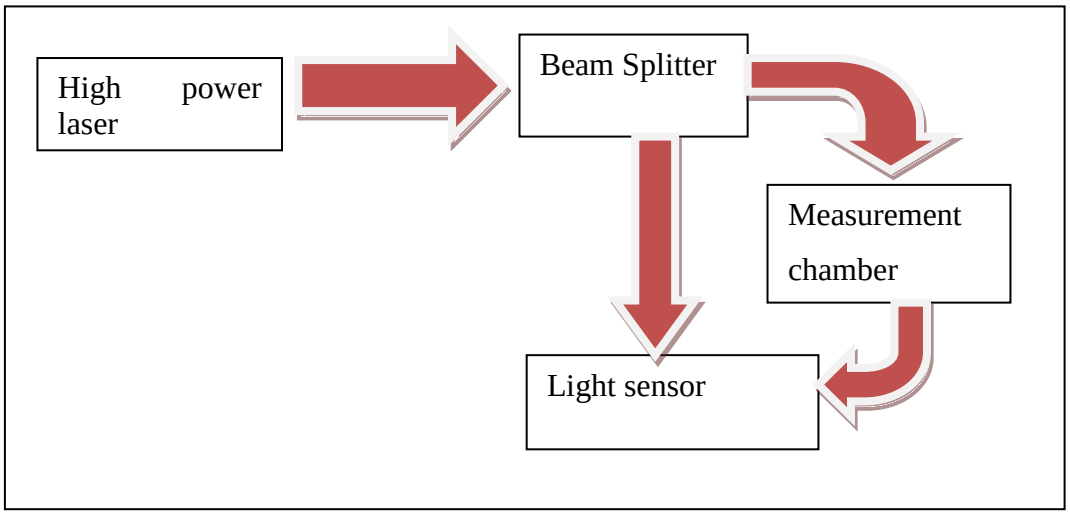

Figure 2.2: The overall system set up for the phase analysis light scattering technique (Corbett et al., 2012). Notice that the laser passes through the sample and a reference to compare frequency shift of the laser source. High power laser is used in the measurement of the electrophoretic mobility.

2.2.2 Coulter counter

Coulter counter method uses electrical signals instead of optical signals for surface charge measurement of biological particles (Takahashi et al., 2011). This method measures the size and distribution of single cells without influence of the shape, refractive index and density. The coulter counter consists of two separated chambers connected by a small channel while solution containing the particles will fill the chambers. The particles will pass through the channel in a singular basis. The electrical resistance of the solution changed when the particle passes through the channel. Changes of the voltage along the channel were detected using electrodes immersed in the solution in each chamber. Electrical pulse in unit of voltage is detected as each particle passes through the channel. The electrical signal will be measure to indicate the size of each particle; while the number of pulses is related to the number of particles. In Figure 2.3, a schematic diagram of the coulter counter is shown. The narrow channel in the middle of the chamber only allows single particles

or cells to pass through the channel. Hence, the measurement is meant for one particle at a time. The result of the measurement is displayed in Figure 2.4. When a particle pass through the narrow channel, the resistance of the channel changes and causes voltage measurement of the channel to fluctuate. The individual spikes displayed in the result (Figure 2.4 (e)) are the single particle signals. The amplitude is the size of the particle. The measurement can be very accurate; however, the measurement needs a long period of time to measure one batch of cells.

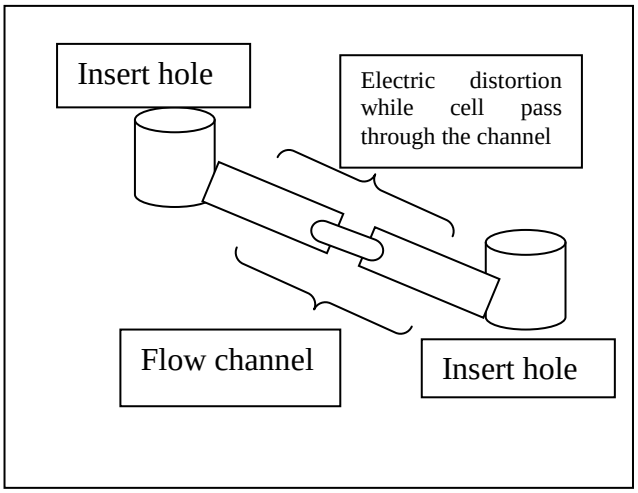

Figure 2.3: Schematic diagram of the coulter counter method (Takahashi et al., 2011)

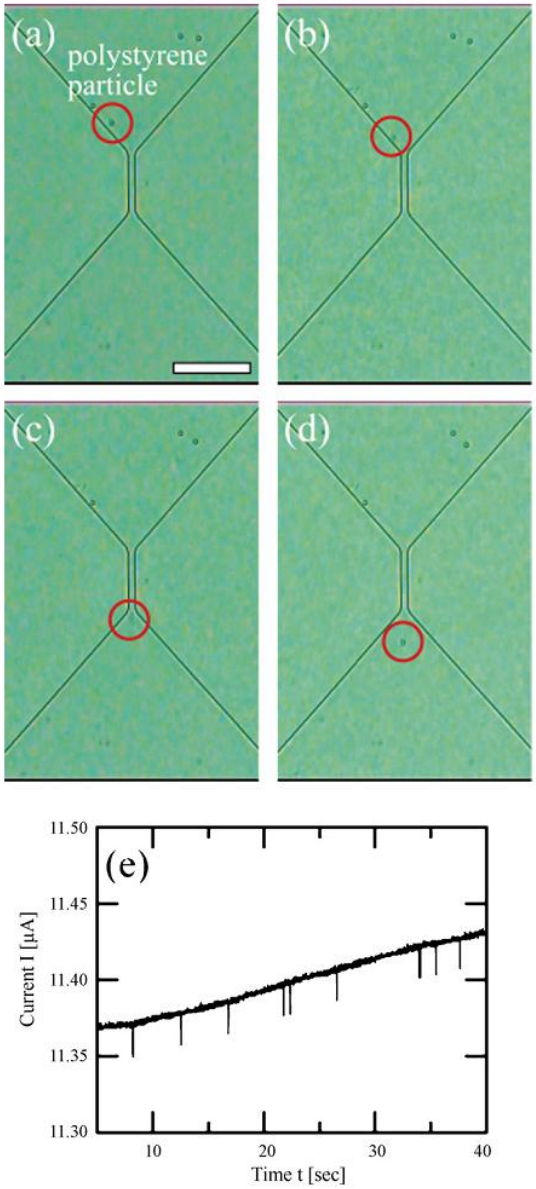

Figure 2.4: (a), (b), (c), (d) The particles are dispersed regularly in the channel, moving towards the channel and through it by being attracted to the applied electric field in the channel. (e) The result of the electric field changes in term of current while the particles travel through the narrow channel (Takahashi et al., 2011).

2.2.3 Suspended microchannel resonator

Surface charge measurement of single particles has been developed by Dextras et al. (2009). This group of researchers used the suspended microchannel resonator (SMR)

for mass measurement and surface charge measurement. This method measures the changes in resonance frequency of a hollow cantilever as suspended particle pass through the cantilever. The total frequency shift is directly propotional to the mass of the particle. Furthermore, the resonance frequency of SMR system is highly sensitive toward the position of the particles in the cantilever. As the particle travel through the cantilever, the resonance frequency change corresponds to the position. The SMR system has demonstrated the ability to quantify the surface charge of particles by measuring the electrophoretic mobility of the particle. The resonance frequency changes are shown in Figure 2.5.

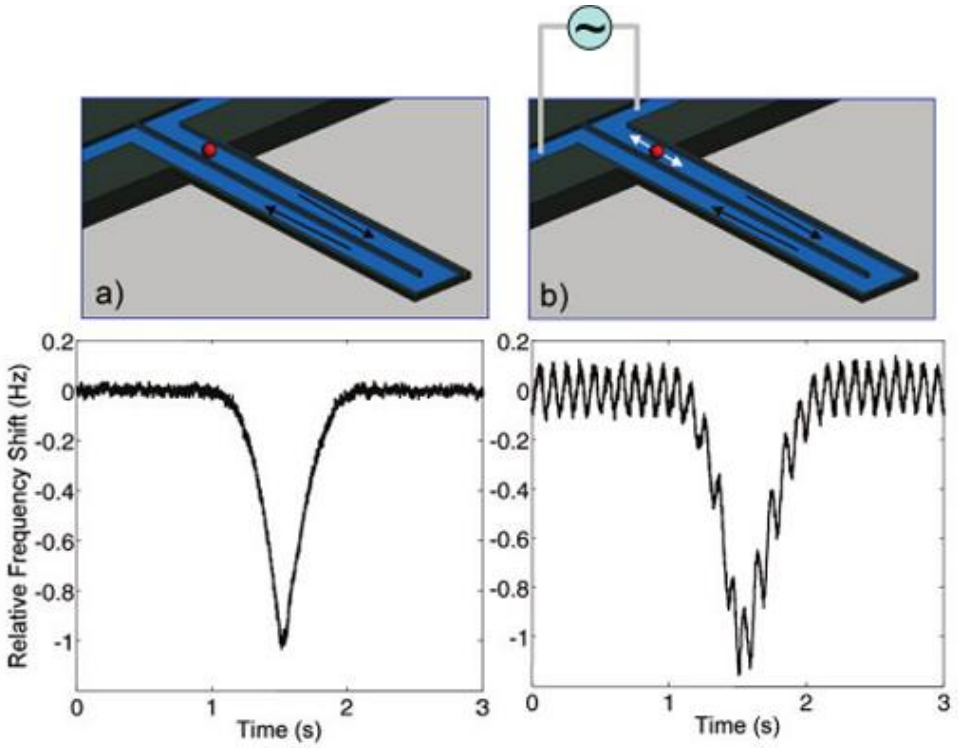

Figure 2.5: SMR uses electrical signal to detect the field distortion as the particles pass through the channel. Surface charge is measure by measuring the distance travelled and time taken for the movement Dextras, Burg & Manalis 2009.

The advantage and disadvantage of the methods was presented in the Figure 2.6. Comparison in between the PALS method, Coulter counters and SMR are presented in term of time of measurement, invasive and display of particle morphology.

	PALS	Coulter counter	SMR
Duration of measurement (per 10 particles)	5 to 15 minutes	10 to 20 minutes	10 to 20 minutes
Invasive (laser damage, pressurize damage)	Yes	Yes	Yes
Display of particle morphology	No	No	No

Figure 2.6: Comparison in between the PALS method, Coulter counters and SMR are presented in term of time of measurement, invasive and display of particle morphology.

2.3 Image processing of cell

Cells are the fundamental units of living organism; they are the primary component of many biological processes. Studies of their physiological process can provide important information about the progression of disease. Ability to observe and define cells' dynamic process in 2 dimensional (space and time) has been achieved by utilising advance imaging technologies (Dormann et al., 2006). These technologies include the segmentation and definition of large number of cells in time-lapse, fluorescent, phase contrast, and intravital microscopy images, making manual analysis a limited option.

The challenges of the automation include bad image quality (high noise and low contrast level), different density of cells (especially when the cells enter and exit the field of view (FOV)), and contact of cells with multiple cells within the same contrast level (Meijering et al., 2009). Many automated cell tracking methods had been suggested and some had successfully commercialized and be published as open sourced software. All this cell tracking methods include three steps: 1. Image acquisition, 2. Cells segmentation, 3. Connection of cells over time.

2.3.1 Image acquisition

The initial point of many investigations of cell movement is to identify the cells' natural behaviour, through recognition of shape changes, direction and persistence of movement. These investigations make extensive use of light microscope, specifically wide field microscopy with phase contrast. The images are collected by CCD cameras as stacks or video. These images will be analysed by image processing, which involves image segmentation, recognising particular behaviours and statistical analysis.

2.3.2 Segmenting individual cells

In the process of cell tracking, it generally consists of two main steps: (1) cell segmentation (separation from background), (2) cell association (recognition of cell in between images). The cell segmentation step is the process of separating an image into important information such as biological part from its background. The result of the segmentation is to provide a new image containing labels indicating which segments of the image represents a single particle and which represents the background. One of the approaches for cell segmentation is using threshold value; in order to label pixels in the images, each pixel of image was compared where the pixels with values above the threshold as particle and values below the threshold as background (Ta et al., 2009). Figure 2.7 shows the post processing result of segmentation from different types of biological particles. This method of segmentation requires well separated cells and their intensity in the images are significant from the background. Initial process of this technique includes image conversion from RGB image to intensity image (shown in Figure 2.8). Other segmentation methods have been proposed for image processing: this includes fitting predetermined cell intensity profiles into image data (Kachouie et al., 2006). But this system only achieves optimum results with images showing constant morphology. However, new strategies of pre- and post processing, such as marking and shape based segmentation has been applied to overcome this issue. Researchers such as Wählby et al. (2004), Yang et al. (2006), Lin et al. (2007), and Zhou et al. (2009) presented the usage of the model based segmentation. These method presented takes

a long period of time for pre and post process of the images captured. Hence it may not be the best solution for real time image processing.

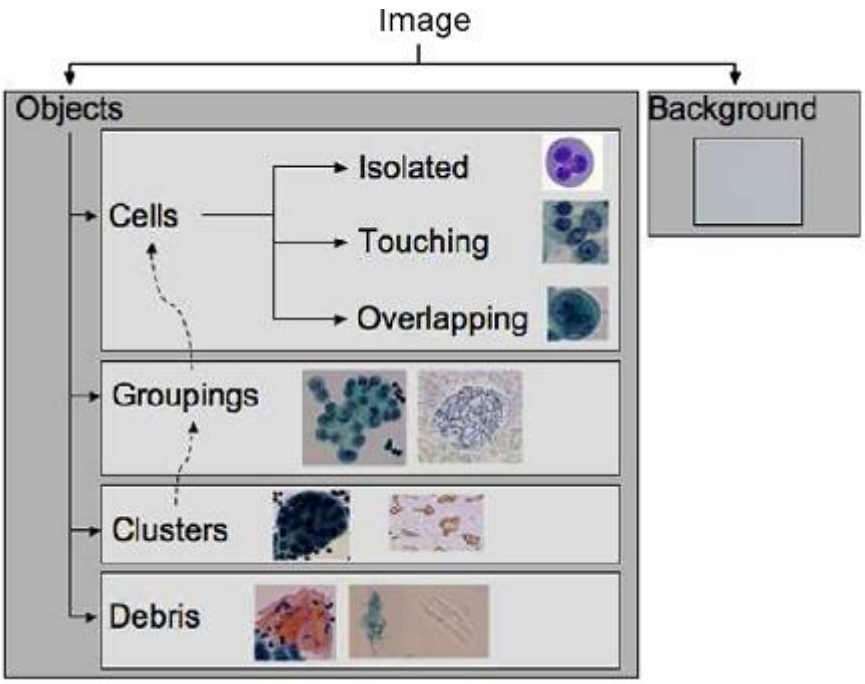

Figure 2.7: Techniques used by image processing programme to differentiate background from targeted cell or particle. Targeted object can be filtered further to analyses the size, group and amount of particles. (Ta et al., 2009)

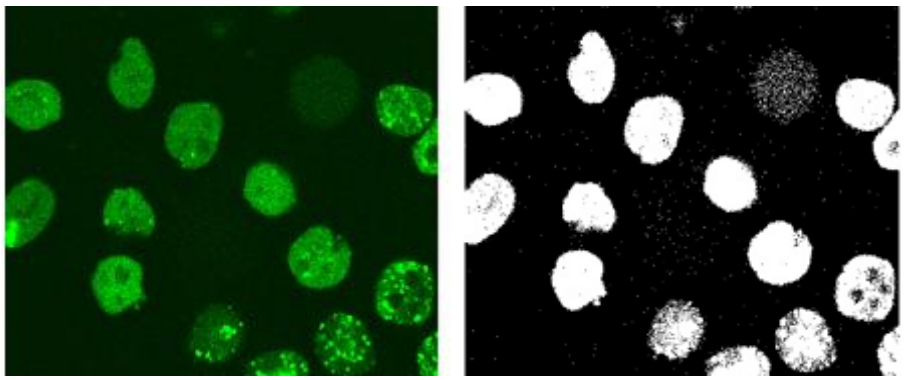

Figure 2.8: Image processing technique used for intensity conversion of the image. The original image with RGB data will be converted into intensity image. Further analysis will be carried out in order to eliminate the cell with size above the threshold value or below threshold value of a normal cell. (Meijering, E. et al., 2009)

After the cell segmentation, the next step for cell tracking is to form a linkage between the cells in images captured at different moment. This refers to the process of identification and synchronizing the segmented cells from one frame to another to obtain the trajectory of the cells. The easiest method to achieve the association is to locate the nearest cell in the next frame and form a link within a predefined range (Debeir et al., 2005; Chen et al., 2009). In order to achieve better accuracy in discrimination of matches, certain parameter can be applied to optimize the process. The parameter includes, reduce the speed of cell movement, similarity in image intensity, volume of cell, perimeter of cell, estimated displacement and boundary curvature. Addition of these parameters for comparison in between frame can reduce the risk of ambiguity. However, additional processing required for these large amount of comparison which will contribute to the long processing time of the data. Hence, we proposed optical flow method which used the comparison of cells average intensity and volume of cells to predict the cells trajectory. The optical flow method assumes smooth movement of cell throughout the whole images, and obtains the cell trajectory. This method reduces the processing period and provides an accurate trajectory measurement.

2.4 Electric Double Layer

Electrophoresis, electro osmosis, streaming potential and sedimentation potential are generally defined as electrokinetic phenomena (Hunter, 1981; Probstein, 1994; Masliyah, 1994). These phenomena happen to a solid surface when in contact with aqueous solution. The local free ions floating freely in the solution will rearrange to produce a region of non-zero net surface charge near the interface. This study focuses on the electrokinetic phenomena caused by the interaction of the applied electric fields, ionic solutions (buffer solution, HEPES) and the diffused layer near solid-liquid interface. Therefore, for the sedimentation potential and streaming potential are not included in the scope of this work. The following session discusses the electrokinetic phenomena, electro osmosis, electrophoresis and all the equation related to the electrophoretic measurement.

When a cell is immersed and by being in contact with an aqueous medium, a surface electrical charge will surround the cell's surface (Camp and Capitano, 2005; Barz and Ehrhard, 2005; Mehrishi and Bauer 2002). The surface charge of a particle can be caused by multiple mechanisms: isomorphous substitution, specific ion adsorption, exposure to charged crystal surfaces, and ionization of surface groups. In the bio-analytical microsystem, the ionization of surface group mechanism plays the most crucial role. In this study, glass was used to fabricate the measurement chamber. Surface silanol (SiOH) deprotonate induces a negatively charged surface and an associated thin diffuse charged layer of ions near the surface. This arrangement between the charges at the solid-liquid interface and the balancing counter ions in the liquid is usually called electrical double layer (EDL). The thin immediate layer of counter ions next to the charged solid surface is called the compact layer (stern layer). The compact layer is an immobile layer which is strongly attracted to the electrostatic force from the charged surface or cell surface. The counter ions surrounding the surface of compact layer are mobile. This part of the double layer is called the diffuse layer (Gouy-Chapman layer). The thickness of the Gouy-Chapman layer is characterized by Debye length which is shown in Figure 2.10. The model of Gouy-Chapman model is shown in Figure 2.9.

When this submerged cell was introduced with applied electric field, the cell migrated toward the polarity of the applied electric field. This movement will produce a sequence of phenomena which are explained in the following section (Electroosmosis and Electrophoresis).

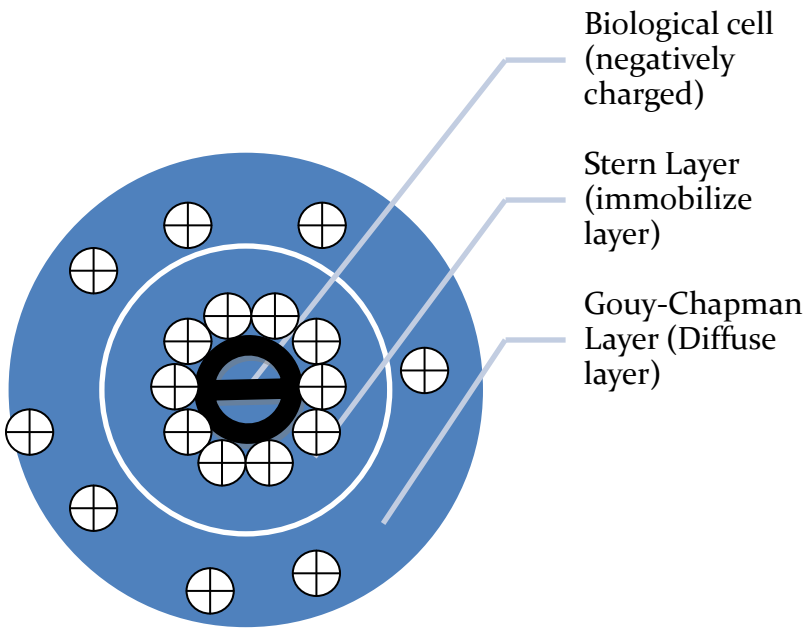

Figure 2.9: Gouy-Chapman model of the electrical double layer. The schematic distribution of the net charge is shown. The biological cell with negatively charge surface is in the middle, the positively charge ion attracted to the cell and it forms two electrical layers. The potential at the interface between Stern and Gouy-Chapman layers is known as the zeta potential.

2.4.1 Electro-osmosis

Electro-osmosis is defined as the motion of liquid relative to an applied potential across a membrane, micro channel or capillary tube. Electro-osmosis flow is caused by the electric potential applied in a solution. When an electric field is applied to a solution, the mobile portion of the EDL will migrate towards the cathode or anode depending on the EDL polarity. The migration of the ions of the EDL promotes viscous shearing of the liquid molecules surrounding the EDL, ultimately resulting in bulk-liquid movement, or electro-osmosis flow. Electro-osmosis flow is independent of the suspended particle size, for cases where the EDL is much smaller than the length of the channel. This phenomenon becomes significant when the channel size is small. The fluid velocity v_{eo} can be defined by equation as shown in equation 2.1.

$$v_{eo} = \mu_{eo} \boldsymbol{E} \tag{2.1}$$

The μ_{eo}, represents the electro-osmosis mobility and *E* as the applied electric field. In this study, channel size is relatively larger in comparison to the cell size, therefore, the electro-osmosis effect on the surface charge measurement were minimal.

2.4.2 Electrophoresis

Electrophoresis is the motion of suspended charged particles, relative to a fluid under the effect of a spatially uniform electric field (Probstein, 1994). Similar to the electro-osmosis flow, the charged suspended cells will migrate towards the anode or cathode depending on the polarity of the particle charge. Figure 2.10 shows the schematic of the electrophoresis system where negatively charged cells will migrate toward the anode of the applied electric field. Counter-ions from the solution are electrostatically attracted to the surface charge of the particle. As the particle migrates through the solution, the counter-ions move in and out of the EDL surrounding the particle. Velocity at which the particle move toward the cathode, relative to the liquid referred to electrophoretic velocity, v_{ep}.

$$v_{ep} = \mu_{ep} E \tag{2.2}$$

μ_{ep} is the electrophoretic mobility and E is the applied electric field.

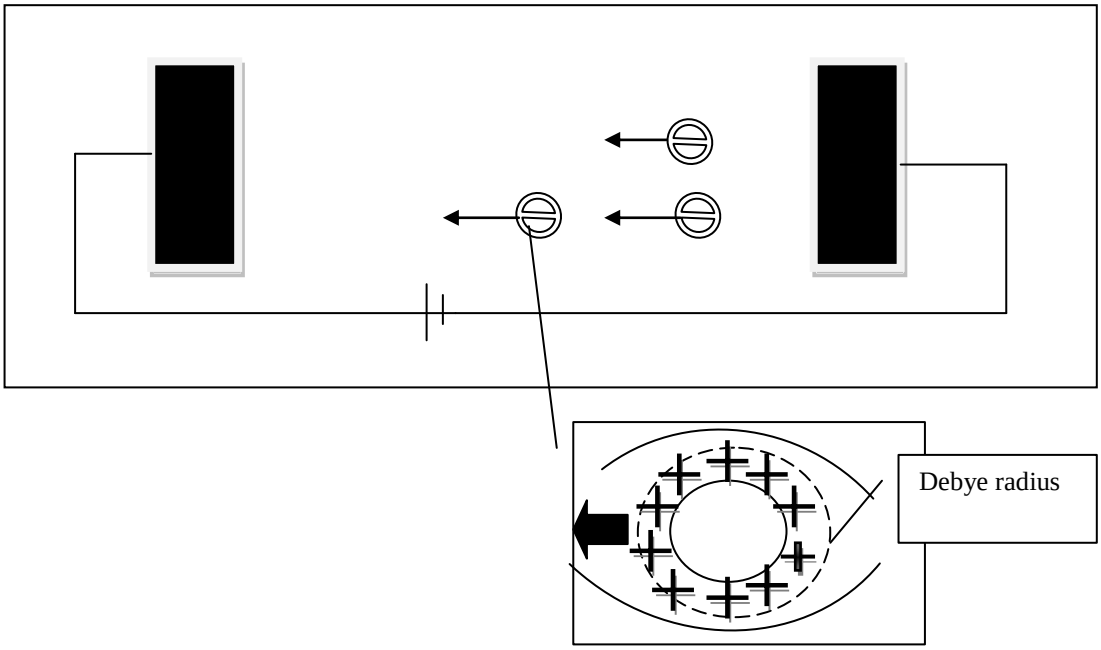

Figure 2.10: A Schematic of electrophoresis, with microsphere or particles. The electrophoresis movement of the particles with negative charge will migrate towards the anode. The microsphere has a relatively small Debye length

2.4.3 Surface charge equation

Electrophoresis and electro-osmosis phenomenon can be expressed in the classical Smoluchowski expression for the electrophoretic mobility of spherical particles. Equation 2.3 represents the EPM as a function of the particles surface potential, ζ, viscosity, η and permittivity, ε of the surrounding electrolyte solution (Smoluchowski, 1918).

$$ = \zeta\varepsilon/\eta \quad (2.3)$$

In the study of cell electrophoresis, many experiments use the equation in Eq 2.3 to calculate the zeta potential with the measured EPM results. However, value of zeta potential varies with the changes opposed by the surrounding electrolyte concentration and therefore, isn't an intrinsic parameter of the cell. The surface charge of a cell is thought to provide better explanation of cell's EPM than the zeta

potential. Since the surface charge of cells is mainly contributed by the ionisable organics substance such as acids and bases. Hence, surface charge of the cell is highly affected by the pH of the electrolyte in the buffer solution which measurement is performed. In consideration of these reasons, it is desirable to calculate surface charge measurement from EPM. The simplest model is given in the EPM formula as follow:

$$\square = \frac{V}{E_0} \tag{2.4}$$

Surface charge of the particle is calculated with the Guoy-Chapman theory (Equation 2.5), where σ is the surface charge and κ is the Debye-Huckel parameter.

$$\square = \frac{\sigma}{\kappa\eta} \tag{2.5}$$

The EPM is directly proportional to the surface charge of the measured particle as shown in Guoy-Chapman theory.

2.5 Surface charge of cell

Cell membrane creates an essential protection or boundaries within the living cell. Cell membrane functions as a separator which separates the interior of the cell from the ambient. It also involves in cell to cell interaction. Any perturbation of cell membrane may affect the surface property and reflect the cell's vitality (Jitendra and Mehrishi, 2002). Surface charge of ion channel proteins enhance conductance, by attracting permanent counter-ions on the ion channel. The surface charge on this channel will separate the other channel via electrostatic repulsion. This will reduce autoimmune responses and protect the channels from protease. This parameter had been introduced to monitor the health status of cells. These alterations can be detected by electrophoresis measurement (Dobrzyn et al., 2013; Piasecki et al., 1997; Poo, 1979; Kremser et al., 2004). The study of the surface charge of cells has been carried out by researchers and cumulated a considerable knowledge bank. These studies find that cells of multicellular organisms have negatively charged surface as

long as they are measured within their natural environment (Figure 2.11). The electrophoretic mobility (EPM) information of various organisms (more than 300 types) indicated that mobility of most cells of multicellular organisms range between 40% and 50% the anodic EPM of human erythrocytes (1.1 μm/s at 1 V/cm) (Slivinsky et al., 1997; Hashimoto et al., 1998).

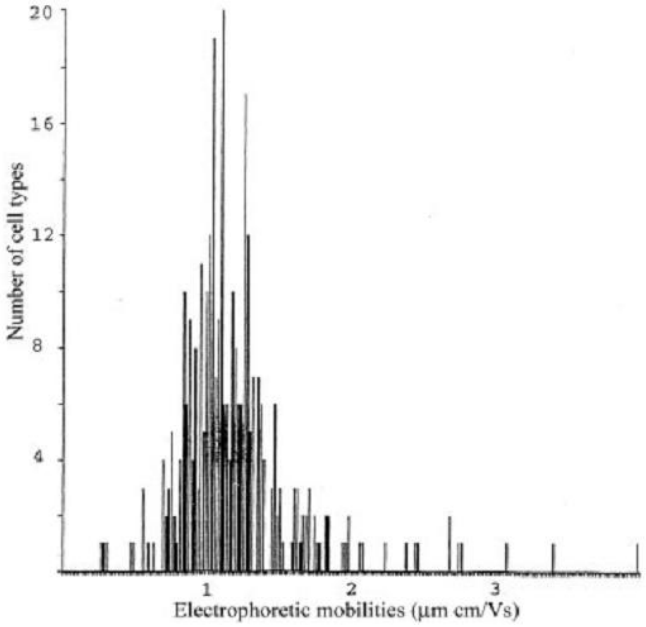

Figure 2.11: The cumulative surface charge data of various kinds of cells from different organisms. The similar data was found in all the experiments done in more than one hundred laboratories by different methods (Slivinsky et al., 1997).

2.5.1 Surface charge of cancer cell

Studies by the group of researchers, Dolowy, 1984, show that the surface charge of biological cells increase during tumorigenesis and decrease during necrosis. The surface properties of malignant cells are different. in comparison to their normal counterparts. Surface charges of the malignant cells possess an unusual cell to cell interaction and are the most essential behaviour for identifying them from their normal counterparts. This application can be apply to identify the prognosis of patient suffering from cancer (Dobrzyn et al., 2013).

The study of the electrical properties in cell membrane during cancer transformation had been carried out by researchers (Dobrzyn et al., 2013). These

studies examine the variation of the electrical charge on cell membranes in an control environment (Szachowicz et al., 2012). One of the results is shown in Figure 2.12. The results are compared between the surface charge of cancer cells and the normal cells. The surface charge of the cancer cell is obviously higher than the normal cell. The surface charge of both cell are different from pH 3 to pH 9. The surface charge of the cancer cell is higher in positive charge in pH 3 and reached isoelectric point at pH 5. The surface charge of cancer cell and normal cell become negatively charge in pH 4 onward. The surface charge of the cells increases and reaches a plateau around pH 7 onward. Graph of the cancer cell surface charge and normal cell surface charge show similar plot pattern. Both cell's surface charge are similarly in plot pattern but cancer cell surface charge is higher compare to normal cell surface charge.

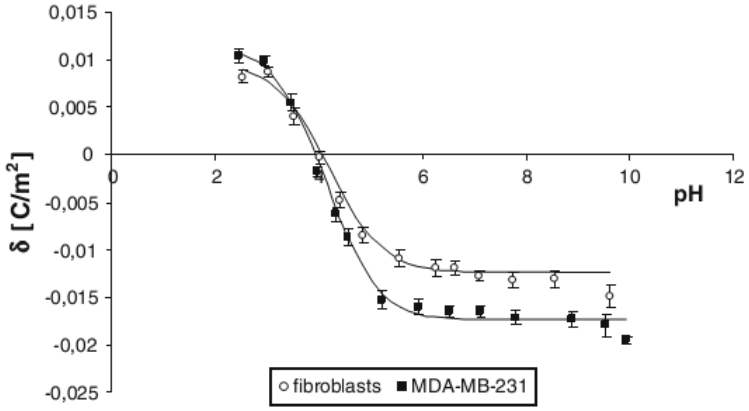

Figure 2.12: Surface charge of cancer cell (MDA-MB-231) and surface charge of normal cell fibroblast (Dobrzyn and Figaszewski, 2013).

CHAPTER 3

METHODOLOGY

3.1 Introduction

The methodology of this study includes four parts. Firstly, the setting up of the compact CCD microscope system, secondly, the image processing system for automated surface charge measurement, thirdly, the surface charge measurement calculation and theory involve and lastly, the preparation of the biological cell (Yeast cell, Human bone cell (hFob 1.19), Human cancerous bone cell (U20s), cervical cancer cell (HeLa) for the surface charge measurement. The details of these four sections are mentioned exclusively in this chapter.

3.2 Experimental apparatus and method

3.2.1 Compact CCD microscope

Compact CCD microscope's overall design is shown in Figure 3.1. The compact microscope is divided into three parts: a) Compact CCD camera, b) Sample chamber and c) Light source. The measurement of the microscope is 13 cm in length, 8.5 cm in width and 15 cm in height. The material for the framework of the compact CCD microscope is aluminium. Aluminium is both light weight and reasonably hard, hence making the CCD microscope extremely convenient as it is easily portable and durable at the same time.

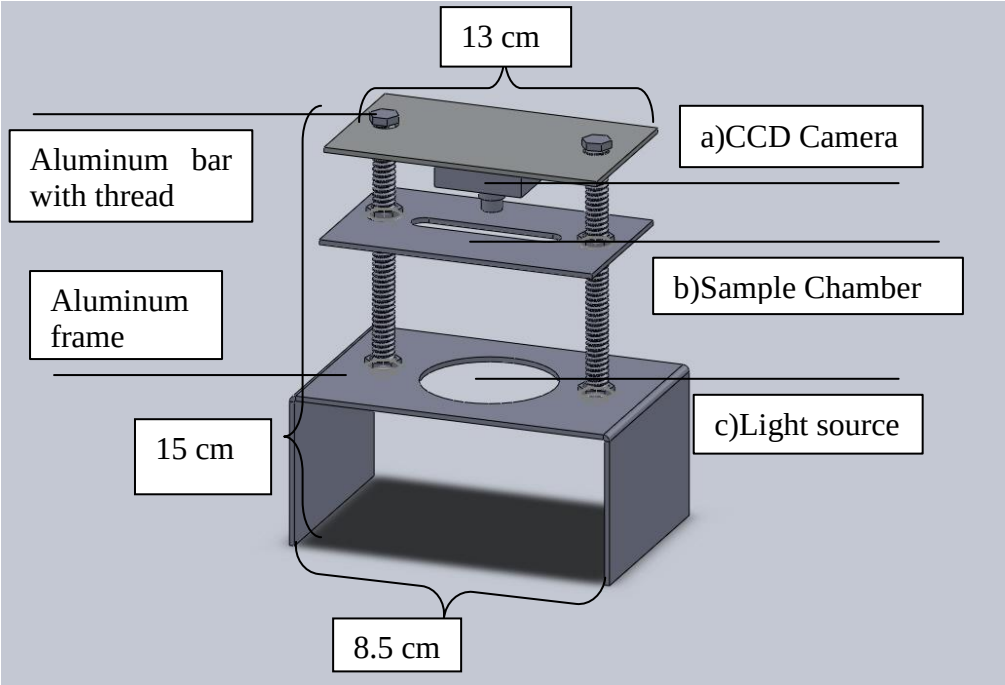

Figure 3.1: Overall design of the Compact CCD microscope, which consist of three parts: a) CCD camera, b) Microelectrophoresis Chamber, c) Light source. The frame of the microscope is made by aluminium.

Compact CCD camera is attached at the top of the microscope as shown in Figure 3.1). The lens of the CCD camera has been inverted and attached with the CCD sensor. This modified lens have numerical aperture (NA) of 1.4 with an effective depth of field of 200 nm. CCD based image sensor with sensor size of 4.386 x 3.64 mm, and resolving power of 640 x 480 was used. The measurement volume is therefore 190 x 160 μm with a depth of approximately 200 nm. This set up allows the magnification of images up to 125 times to focus on the CCD sensor for image acquisition. Images acquired are sent directly to a computer for further image processing.

The sample chamber is placed in the middle of the microscope. Sample chambers provide the holder to hold a sample during surface charge measurement. The sample chamber is built with an empty hole in the middle of the chamber to allow light to project towards the sample. Sample chamber will hold the microelectrophoresis chamber which will provide the measurement platform for

the experiments. This setup allows the camera to capture the image of viable samples with back illumination from the light source.

The third part of the compact microscope is the light source. Light source is placed at the bottom of the microscope. The light source is provided by a 5W Hi-power LED with emission wavelengths of 460 nm. In addition, a collimator lens (with NA of 0.50) is inserted in the optical path between light source and the CCD camera to align the light emitted from the LED.

3.2.2 Microelectrophoresis chamber with two electrodes

Schematic of the microelectrophoresis chamber is shown in Figure 3.2. The material of the chamber is made of borosilicate glass with a rectangular cross section (0.2 cm x 0.5 cm) with a length of 2 cm. Two copper electrodes was attached to the end of the chamber. This chamber serves as a holder for the microelectrophoresis system, where HEPES solution with suspended cells could be injected into the empty gap of the chamber. The DC power supply will then provide the applied electric field to the chamber via copper electrode for surface charge measurement.

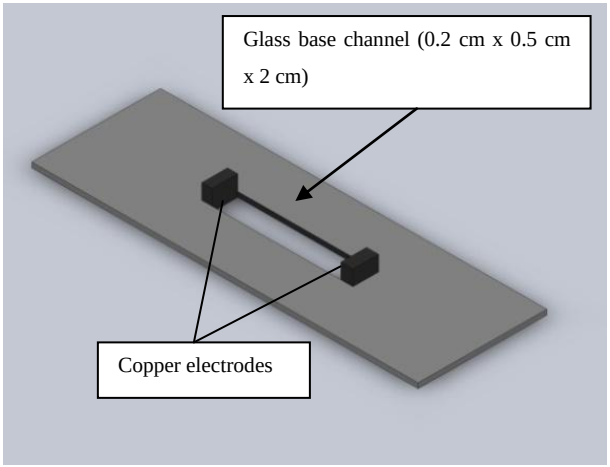

Figure 3.2: Schematic of the measurement chamber. A glass base channel was made with a rectangular cross section (0.2 cm x 0.5 cm) and a length of 2 cm in middle of the chamber. The channel is covered with a thin glass during surface charge measurement.

3.2.3 DC power supply

DC electric field is applied using a voltage power supply (M10-TP3003, MCP lab electronics, MY). The power supply is used to apply steady voltages from 5 V, 10 V, 15 V, 20 V, and 25 V to the copper electrodes, which are inserted at both ends of the glass channel to create a steady DC electric field across the channel.

3.3 Imaging system

The overall experimental setup for this study is shown in Figure 3.3. The flowchart shown in Figure 3.3 illustrated the cells tracking process which consisted of experiments, automated processing, and result display steps. MATLAB is used to acquire, process, and display the image captured with an identified cell and surface charge measurement.

3.3.1 Calibration of the compact CCD microscope

Magnification of the system is made constant throughout the measurement process. Calibration of the magnification is carried out with polystyrene beads sized 10 μm ±

5%. The image of the polystyrene bead is captured, and then the size of the polystyrene bead is converted into pixels. The magnification value is constant as the same system with the same parameter are used (magnification lens, distance between sample and lens, and same CCD base camera).

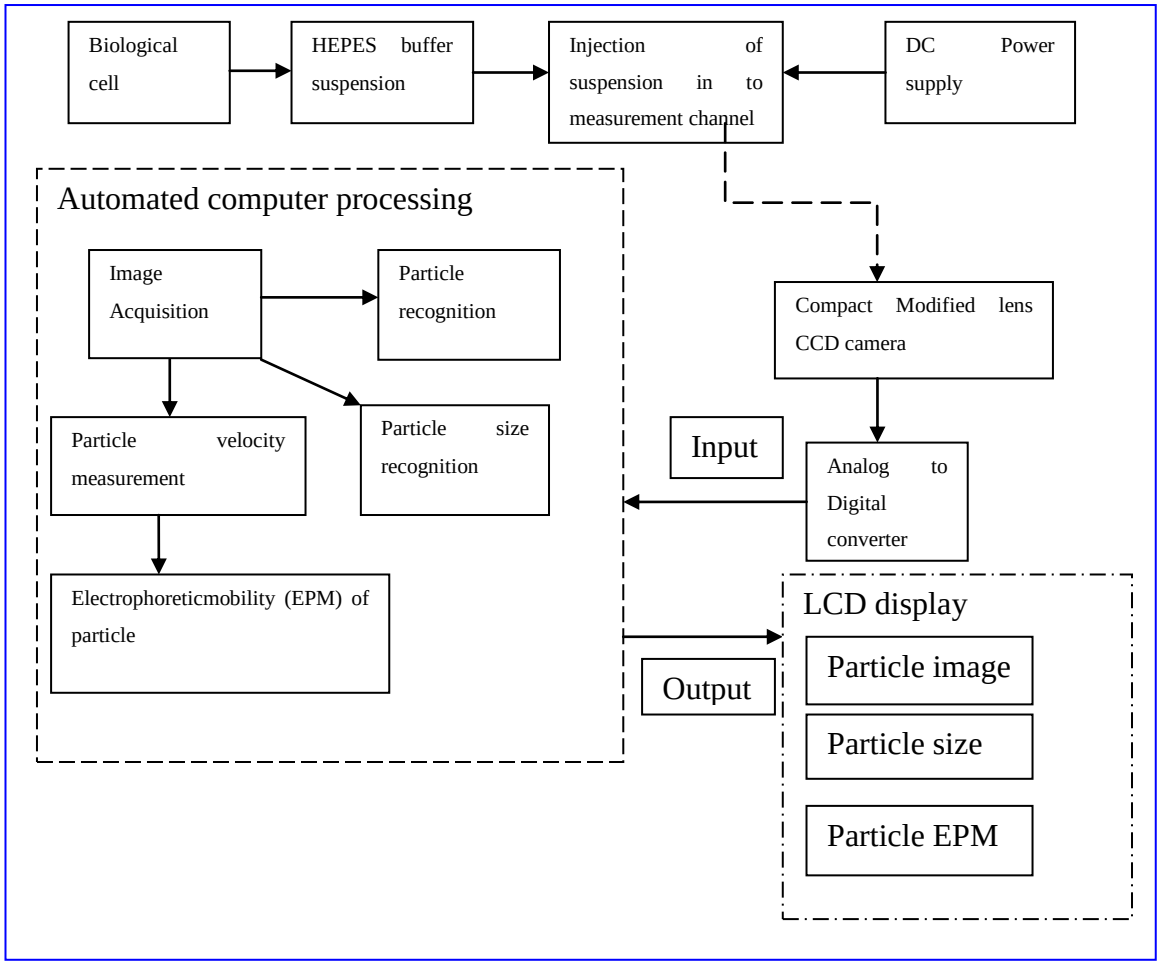

Figure 3.3: Overall experiment setup in this study. Biological cells' images were captured using a CCD base microscope. In the measurement process, electric field was applied by the power supply to the electrode in the measurement chamber.

3.3.2 Experimental procedure and image data collection

In the experiment, cells displacement in DC electric field was measured by capturing 30 sequential cell images, using exposure time of 10 ms and a frame rate of $\Delta t = 66.7\, ms$. Biological cells such as yeast cell, normal bone cell, cancerous bone cell and cervical cell were used. Moment before loading the measuring chamber with the

cell suspension, HEPES solution is flushed through the channel to prepare the surface for the electrophoretic flow experiment. In all the experiments tested here, HEPES solution is used as the background electrolyte. Before the samples are injected into the chamber, the pH of the HEPES solution is measured and recorded. The pH values are measured using a pH meter (PB-11-P10, Satorius, PB series) and the HEPES solution pH value range was recorded as pH 4 to 8 (range from 4, 4.5, 5, 5.5, 6, 6.5, 7,.7.5, and 8). The cells density and suspension is measured at approximately 3×10^3 cell/ml. An example of the yeast (image) is shown in Figure 3.4. Individual cells will be track and the measured surface charge will be displayed. Images of cells are captured 5 µm above the measurement chamber to ensure the displacement had a negligible parameter as a result of pressure driven flow (due to slight electrostatic force on the glass surface of the measurement chamber). In this experiment, in order to reduce the joule heating effects, the electric field was only applied in 10 seconds burst. The images of the cell will be captured 1s after the application of electric field, this 1s delay ensures that the displacement of cells are measured in a fully developed electro-osmosis velocity field.

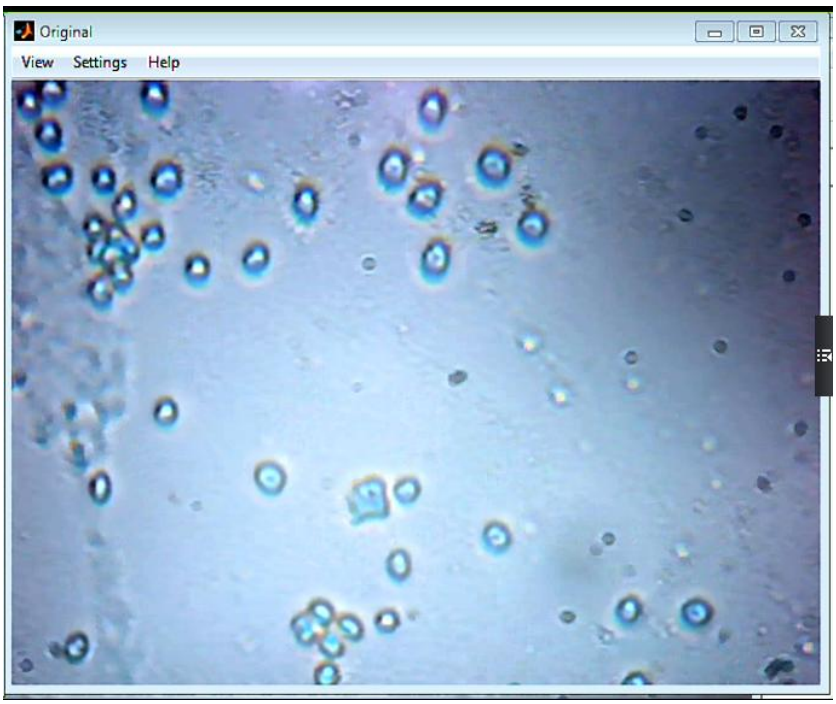

Figure 3.4: Image of yeast cell captured using the CCD microscope in the microelectrophoresis system.

3.4 Data Analysis

3.4.1 EPM and surface charge measurement

All the cells are assumed to have a unity of specific gravity; hence the buoyancy force is negligible. Same goes to the Brownian motion, the Brownian displacement are minor compared to electrophoretic displacements in the measured condition hence, Brownian motion is neglected.

Before considering the form of an electrophoretic term, it is important to consider the charged relaxation processes and the scales of time related. The interested subject here is the transient motion of the cells when there is a sudden change of electric field. The inertial response time (T_p) of the cells may be estimated to be of order

$$O(\alpha^2 \rho/\eta) \tag{3.1}$$

where (α) is the cell radius, (ρ) is the cell density, and the absolute viscosity of the buffer solution (η). In this study, the diameter of cells used have a diameter of 4 µm: the inertial response time $T_p = O(10^{-6})s$. The applied DC electric field will provide a steady state of electrophoretic displacement, the electric charge function in our study is T. Since, T is much bigger than T_p, we assumed the inertial response of the cell are not observable. The time for the electro-osmotic velocity to become stable and constant may be calculated at $T_{eo} = O\left(D_h^2 \rho_f/\eta\right)s$ (Lopez-Garcia et al., 2000), where D_h represent the inner diameter of the channel and ρ_f represent the density of the fluid used as buffer solution. In this study, the channel, $T_{eo} = O(10^{-4})s$. The local fluid velocity will be steady, if the images of the cells were captured at time greater than T_{eo} after the application of the electric field. We have concluded that the expression $v_{ep} = \mu_{ep} E$ can be used where E is the electric fields for the voltage of interest (v_{ep} is the Electrophoretic velocity of the particles, μ_{ep} is the Electrophoretic mobility of the particles).

From the image processing process, the result of the velocity will be calculated after the cells are identified. It begins with identification of the same labelled objects in between two images, this relation of the same particle over time depend on the optical flow algorithm,

$$E = \iint \left[\left(I_x u + I_y v + I_t \right)^2 + \alpha^2 (\|\nabla u\|^2 + \|\nabla v\|^2) \right] dx\, dy \tag{3.2}$$

$$E = \iint \left[\left(I_x u + I_y v + I_t \right)^2 + \alpha^2 \left(\left(\frac{\partial u}{\partial x} \right)^2 + \left(\frac{\partial u}{\partial y} \right)^2 + \left(\frac{\partial v}{\partial x} \right)^2 + \left(\frac{\partial v}{\partial y} \right)^2 \right) \right] dx\, dy \tag{3.3}$$

I_x , I_y and I_t are the spatialtemporial image brightness derivatives

u is the horizontal optical flow

v is the vertical optical flow

E is the velocity field

$\frac{\partial u}{\partial x}$ & $\frac{\partial u}{\partial y}$ are the spatial derivatives of the optical velocity component *u*

α is the global smoothness term.

Then, the optical algorithm will compute the average velocity of the identified particles in the image. The identification of the cells will depend on the spatial/temporial image brightness of the labelled cell. The technique is further simplified by the Horn Schunck method for minimum coputation time. Horn Schunck method minimizes the velocity field to:

$$u_{x,y}^{k+1} = u_{x,y}^{-k} - \frac{I_x \left[I_x u_{x,y}^{-k} + I_y v_{x,y}^{-k} + I_t \right]}{\alpha^2 + I_x^2 + I_y^2} \tag{3.4}$$

$$v_{x,y}^{k+1} = v_{x,y}^{-k} - \frac{I_y \left[I_x u_{x,y}^{-k} + I_y v_{x,y}^{-k} + I_t \right]}{\alpha^2 + I_x^2 + I_y^2} \tag{3.5}$$

$\left[u_{x,y}^{k}, v_{x,y}^{k} \right]$ is the velocity for the pixel at (x, y). For *k*=0, the initial velocity is 0. $\left[u_{x,y}^{-k}, v_{x,y}^{-k} \right]$ is the neighborhood average velocity. Magnitude of the resultant velocity, *v* will represent the velocity of the cells in between two images. The average results

of the cells' velocity will be measured with a time frame of 9 seconds as the applied electric field will be off after 9 seconds of image acquisition.

After the average velocity values are obtained from the image processing, the velocity was use in the equation of electrophoretic mobility (EPM) (Eq 3.6). The velocity is proportional to the applied electric field strength, E_0 (Smoluchowski,1918). The surface charge was obtained by dividing the velocity of the biological cell with the electric field of the chamber.

$$\propto = \frac{V}{E_0} \tag{3.6}$$

Where $\propto$, is the electrophoretic mobility of the cells, V is the average velocity of the cells measured using image processing method. Obtaining the value of the EPM, the surface charge of the cells are determined by using the Gouy-Chapman theory (Eq 2.5). In this study, all the experiments are carried out with the same type of buffer solution (HEPES), the viscosity of the solution is constant throughout the experiment. From the equation 2.5, the EPM is directly proportional to the surface charge; therefore we displayed the EPM value to indicate the surface charge of the measured particle.

3.4.2 Electrokinetic Transport Equations

This section illustrates the set of conservation equation including fundamental equations of electro-kinetic transport phenomenon. The chemical reactions that takes place in this system are presented as *i* type.

The *i* type of component associated with the mass transport may be written as,

$$I_{i\rho} = \rho_i v_i \tag{3.7}$$

where ρ_i is the density of the component, and v_i is the velocity of the component. Conservation of mass for *i* type states that,

$$\frac{\partial \rho_i}{\partial t} + \nabla \cdot \rho_i v_i = r_i \tag{3.8}$$

Where r_i represents the mass flow rate at which types are produced or consumed. In the fluid mixture with a homogeneous composition, the conservation of mass can be represented as:

$$\frac{\partial \rho}{\partial t} + \nabla \cdot \rho v = 0 \tag{3.9}$$

For a constant and regular density fluid, Eq 3.3 can reduce to:

$$\nabla \cdot v = 0 \tag{3.10}$$

3.4.3 DC electric field displacement

In the DC electric field, the derivation of the particle displacement is simple. For a static DC electric field $E_{DC} = \{E_{DC}, 0,0\}$ the electrophoretic velocity is

$$\boldsymbol{u}_{ep,DC} = \mu_{ep} E_{DC} \tag{3.11}$$

The velocities of the particles are in the direction of the applied electric field. The μ_{ep} is the real-value and identical in magnitude and signed to the respective electrophoretic mobility. The cell velocity and the direction of the mobilities are determined by the DC electric field. The DC displacement was compute at an impression which integrate with a finite time Δt ,

$$X_{DC} = \mu_{ep} E_{DC} \Delta t + C \tag{3.12}$$

The constant *C* determines the initial location of the cell. The cell displacement, X_{DC} Will be measured using image processing method with optical flow technique (step by step image processing method shown in Figure 3.5). The image processing part for acquiring the electrophoretic mobility will be discussed in section 3.3.

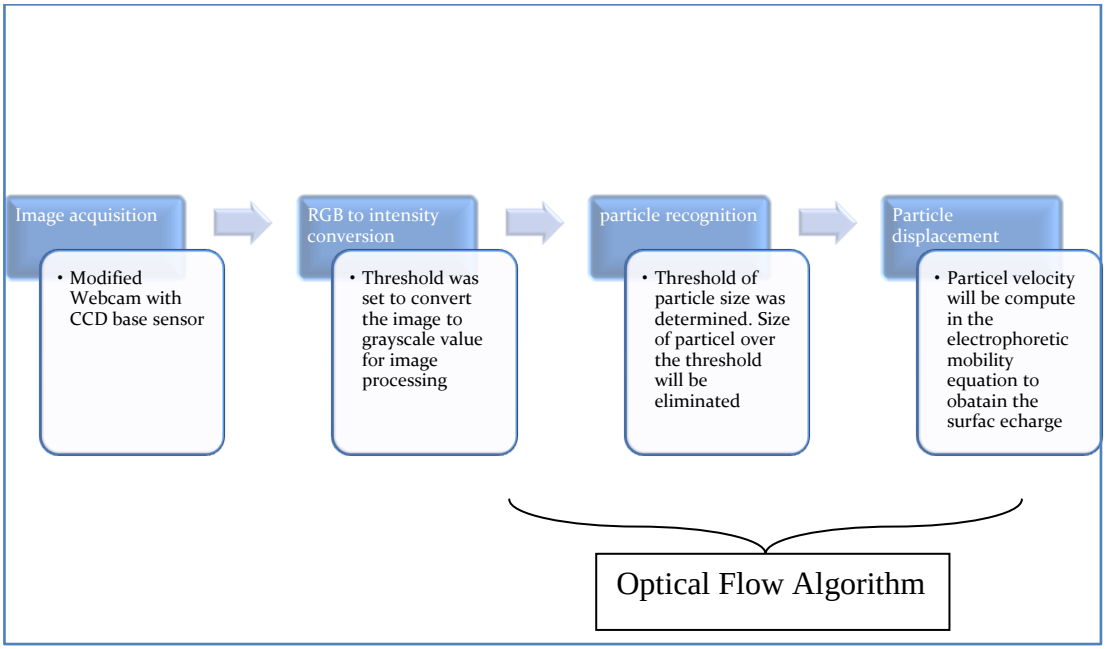

Figure 3.5: Flowchart showing the major image processing method used in surface charge measurement. The results of this image processing are particle velocity. This result will be further process to obtain the surface charge of the cell.

3.4.4 Image processing

A Custom particle tracking programme written in MATLAB was used to measure the two-dimensional displacements and velocity of biological cells in an applied electric field. The overall MATLAB programme of the image processing was shown in Figure 3.6.

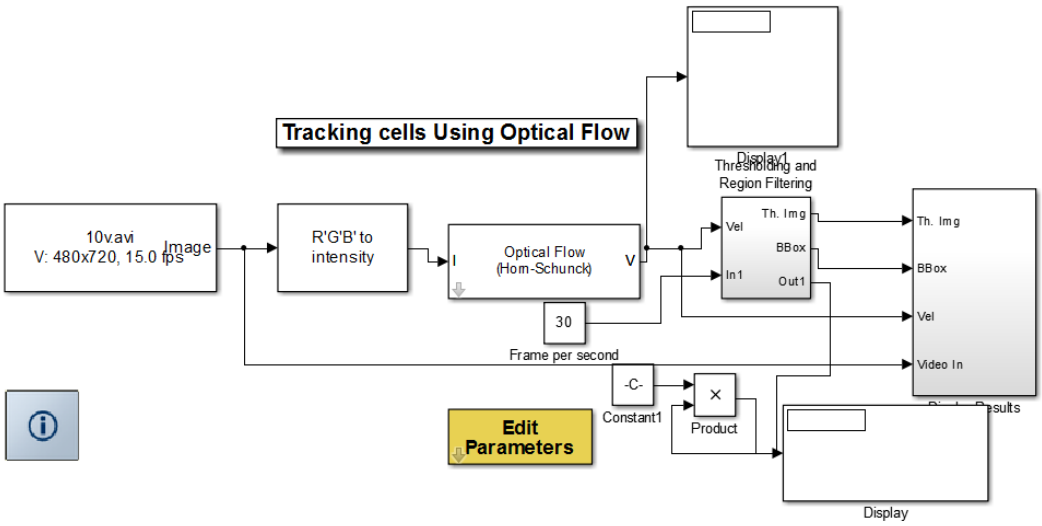

Figure 3.6: Summary of the custom programme used for the automated image processing of the captured image. The process started with image acquisition from the most left box, pass the image to image data conversion (RGB to intensity)

The raw images acquired by the compact CCD microscope mentioned in section 3.2 (Figure 3.4), was sent for intensity conversion, in order to remove spatial noise. The process started with the function of "Red Green Blue" colour (RGB) to intensify the conversion. This function was programmed to convert colour information between colour spaces. The raw images with colour information were converted to intensity information. Idea of performing this step is to differentiate the background from the targeted particles. In the intensity mode as displayed in Figure 3.7, the back ground intensity is different from the particle intensity. The targeted particles will have a high intensity perimeter which will form a ring or a complete figure in comparison to back ground intensity. Using this feature, the programme can further analyse to eliminate the background noise.

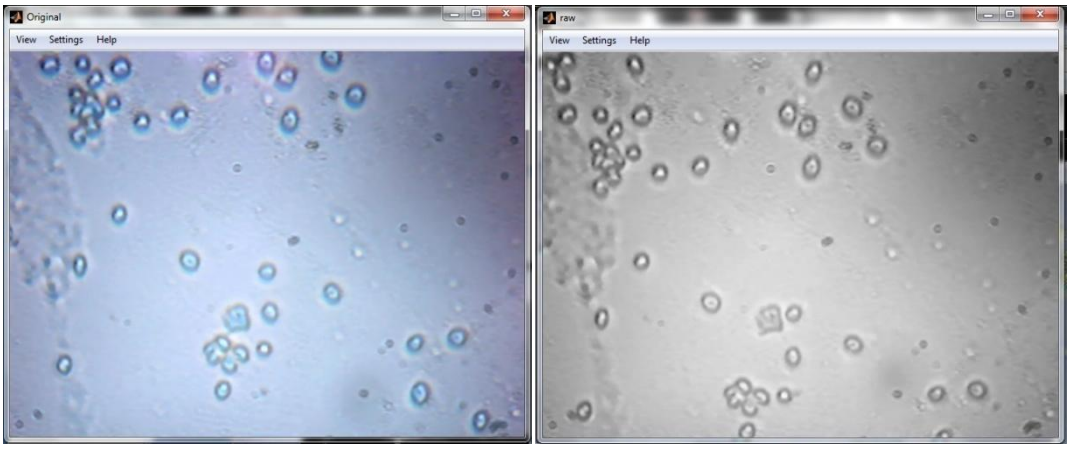

Figure 3.7: Using the RGB to intensity conversion function, the raw images are converted to intensity base image. The intensity of the particles and background can be differentiating at this point. In the image, the particles have a high intensity edge around the perimeter.

After obtaining the intensity value of the image, the image will be passed to the function of filtering. The image is then filtered and processed into binary image. Beside of the binary conversion, this filter also functions to eliminate the particle that was above or below the threshold size. The elimination process of the filter function is to search for linkage of intensity pixel to the neighbouring pixel. The distance of the neighbouring pixel is set to three pixels. Any pixels with the same intensity in between three pixels away will be recognised as linkage. Once the linkages in between pixels form a close perimeter, it will be recognised as a valid particle.

In this study, experimentation of biological cells is carried out in homogenous type of cells hence, the size of the cells are almost constant. Larger particles that are detected are coagulated while the smaller particles are debris or lyses. By using this function, the error of measuring unnecessary cells can be reduced. The result of the filter function is display in Figure 3.8. The white coloured particles are identified particles while black colour regions are the background medium. Then, morphological operation was performed to remove stray outliers (small particle). After filtering the number of stray data, the image is then dilated by convolving the cell's binary image with the kernel,

$$\begin{pmatrix} 0 & 1 & 0 \\ 1 & 1 & 1 \\ 0 & 1 & 0 \end{pmatrix}$$

Convolution process will smoothen the regions with cells, effectively removing any unintended isolated pixels caused by noise in the image background. Individual cells identified are then labelled and sorted along pixel rows due to the displacement is ultimately oriented along the horizontal axis.

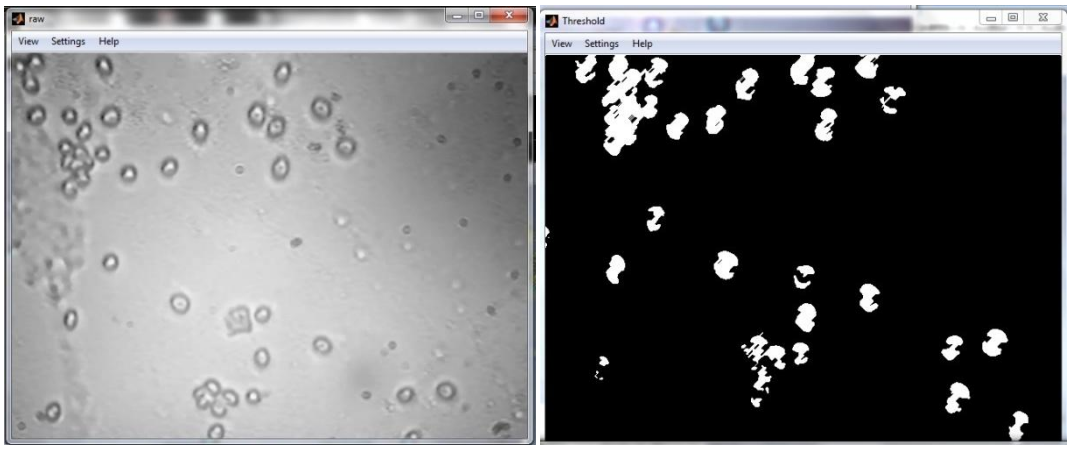

Figure 3.8: Filter function converted the image's intensity into binary based image. Particles that are recognised in the image form a close perimeter with the neighbouring pixels. Particles with larger pixels or smaller pixels will be eliminated.

After obtaining the binary image of the tagged particles, the image will be sent to the region filtering function. This function is customised to determine the movement and direction of the particles from one frame to another. The direction of the individual tagged particles will be display as shown in the Figure 3.9 with the yellow line as an indication of its directed movement. The movement of these particles will then be determined by comparing two images with temporal difference. As the tagged particles are already recognised by the programme, the displacement from one image to the next image can be determined. Then, the directions of particles' movement will be labelled using yellow lines as the indicator. Longer lines represent larger displacement and vice versa.

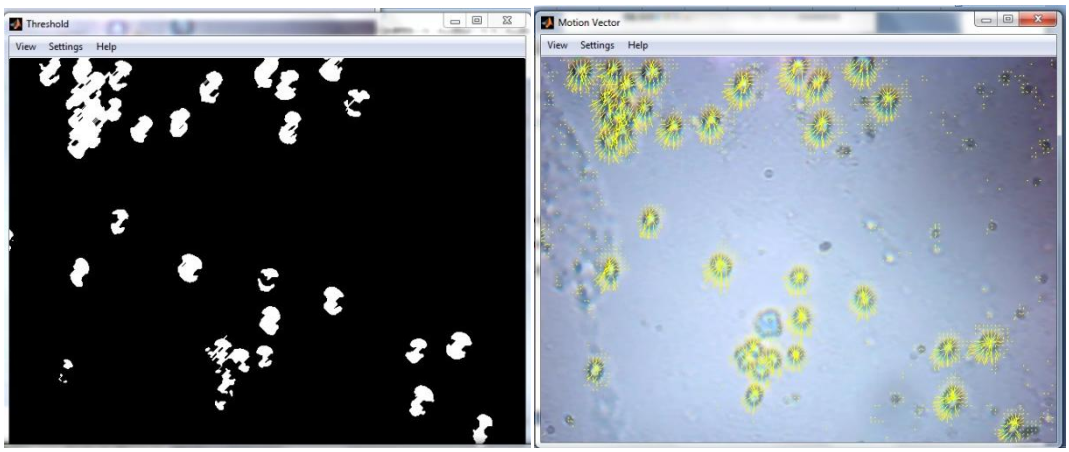

Figure 3.9: The binary image with tagged particles will be processed using the region filtering function. The result of the function is displayed with the direction of movement. The particle with higher movement will have a longer vector line. Shorter lines indicate less movement of particle in between images.

At the same time, the image processing continues with the function of drawing green blocks around cells that have been identified. This green block indicates the number of cells that were measured by the system. The number of the cells is displayed at the right corner of the same display window (Figure 3.10).

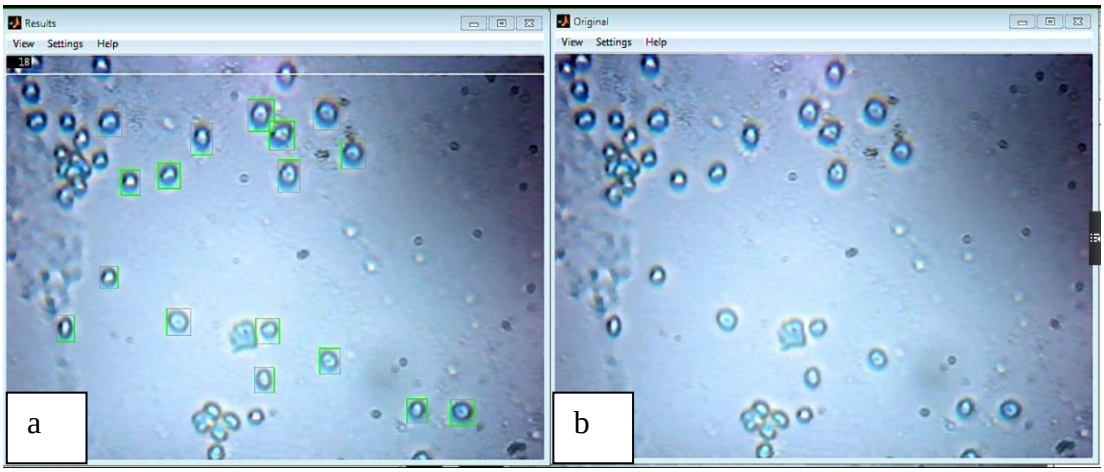

Figure 3.10: Examples of images captured using modified webcam. a.) Image from the MATLAB image processing result, with green boxes indicating individual cells and the amount of cells shown on top of the window.
b.) Original image captured and displayed in real time.

3.5 Biological Cell Preparation

The biological cells of yeast, normal bone cells (hFob 1.19), cancerous bone cells (U2OS), and cervical cancer cells (HeLa) are cultured in this study. Yeast (control) as one of the selected biological cells in this study, provides an easily prepared feed stock to be used to investigate the surface charge measurement.

On the other hand, cancer cells are chosen as biological cell sample. In year 2012 alone, cancer contributed to the death of almost 14.6% of humans globally (WHO, 2014). It has drawn a great interest of researchers to search for new techniques for early diagnosis of cancer formation. In this study the surface charge of normal bone cells in comparison to cancerous bone cells are investigated. Study on the surface charge of normal and cancerous bone cells is to find the difference in the surface charge between these two cells. The surface charge can be used as an early detection of cancerous formation in human cells.

3.5.1 Yeast cell

Yeast cells are cultured and suspended in HEPES solution (Kaysinger and Ramp, 1998) which has the concentration of 1 M. The buffer solution is prepared by adjusting the pH value of the solution using dilute acid (1M HCl) and alkali (0.5 M NaOH). Overall, buffer solutions with pH value of 4 to 8 (4, 4.5, 5, 5.5, 6, 6.5, 7, 7.5, and 8) are prepared. The yeast is added to the buffer solution and stirred with a moderate speed. This process will allow yeast cell to disperse regularly in the buffer solution. After that, the yeast cell will be transferred from the mixing veil to the compact CCD microscope for surface charge measurement. The yeast cell can be prepared anytime via a simple procedure.

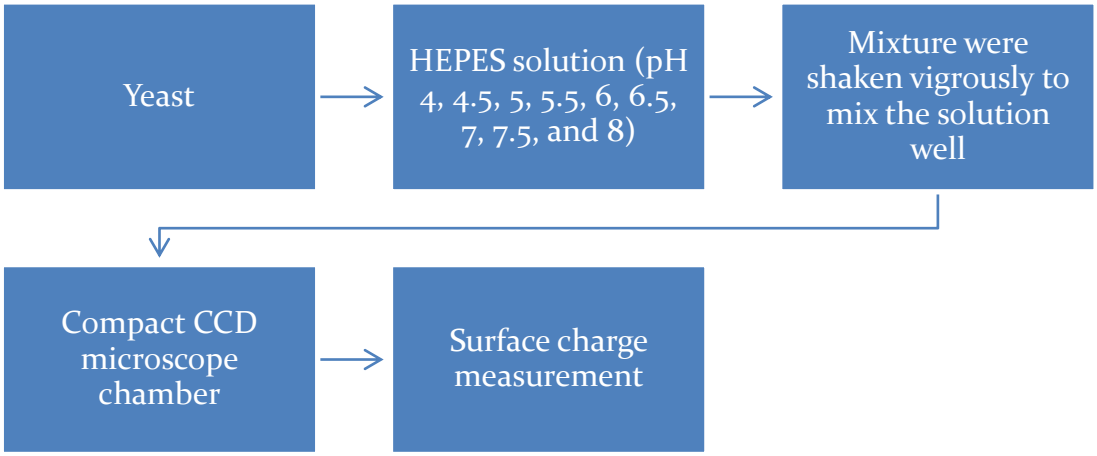

Figure 3.11: Process of preparing yeast cell for surface charge measurement.

3.5.2 Cell culture procedure

The step for culturing cells with modified medium once every two days is shown in Figure 3.12. This step can be applied for all types of cell culture and tissue, provided with the correct medium used for specific cell type. The volume of the culturing flask used for this study is 75 cm^2. Firstly, the old culture medium which contains waste product from cells is removed using a 1 ml pipette. Then the flask was rinsed to remove all traces of serum which contains tripsin inhibitors. Solution used for the rinsing process is 0.25% (w/v) Trypsin- 0.53 mM EDTA solution. After that, Trypsin- EDTA solution (2.0 to 3.0 ml) was added to the flask. Cell in the flask will start to dispersed and detached from the flask wall. The cells were observed using an inverted microscope until all the cells are fully dispersed (usually within 5 to 15 minutes). Then, 6.0 to 8.0 mL of complete growth medium is added into the flask and aspirate cells by gently pipetting. This slows and gently motion will prevent the cells from clumping. Finally, this medium with suspended cells is transferred to a new flask. 2 ml of the mixture will be transferred to each new flask, and then the additional medium will be added to achieve the optimum level for the 75cm^2 flask

limit. The maximum amount of medium is then added to encourage the growth of the cells. The flask will later be transferred into an incubator with a constant temperature of 34^{o}C for incubation. The incubator with 5% of CO^{2} will provide the optimum environment for the cell growth. Normal cells and cancer cells need the same optimum condition which simulates the condition of the human body.

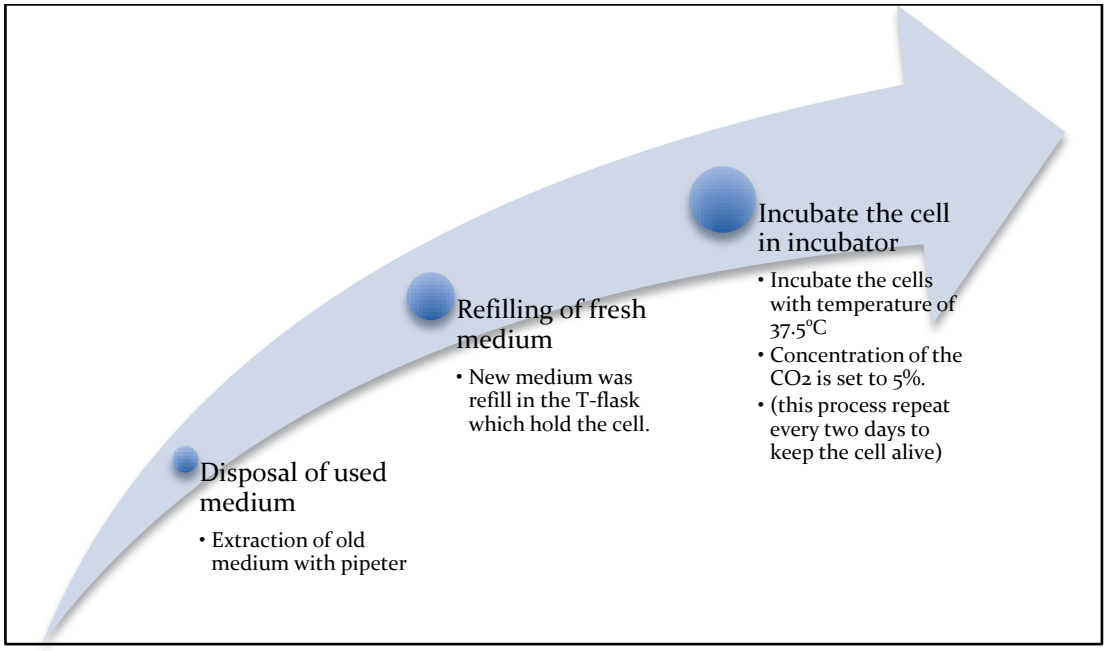

Figure 3.12: Process of Cell culture which carries out for all cell line in this experiment.

3.5.3 Normal human bone cell (hFob 1.19)

Normal human bone cells (hFob 1.19) are from ATCC (Harris and Spelsberg, 1997). The culture medium used for this cell line is a mixture of Ham's F12 Medium Dulbecco's Modified Eagle's medium (DMEM) with L-glutamine. The complete growth medium, consist of the following components in the base medium: 0.3 mg/ml of G418 and 10 % of fetal bovine serum added to a final concentration.

Cell culture starts with thawing the frozen cell line. The thawed cell line will be transferred into the culturing flask for rejuvenation purposes. Cell medium will be changed once every two days to maintain the nutrients needed for the cell growth.

Bone cell is an adhesive cell type, therefore the cells will start to get attached to the bottom of the flask (day 6 in Figure 3.13). Due to the adhesive nature of the cell, liquid tripsin EDTA is used to detach the cells from the flask in order to subculture the cell line. The same procedure is applied in the process of collecting the cells from the flask for surface charge measurement. Normal bone cell line takes around 14 days to double in the amount of cell. Therefore, the subculture process is carried out every fortnight and cells are collected for surface charge measurement. The procedure for the culture is mentioned in section 3.5.2. The temperature for this cell line is 34^{o}C.

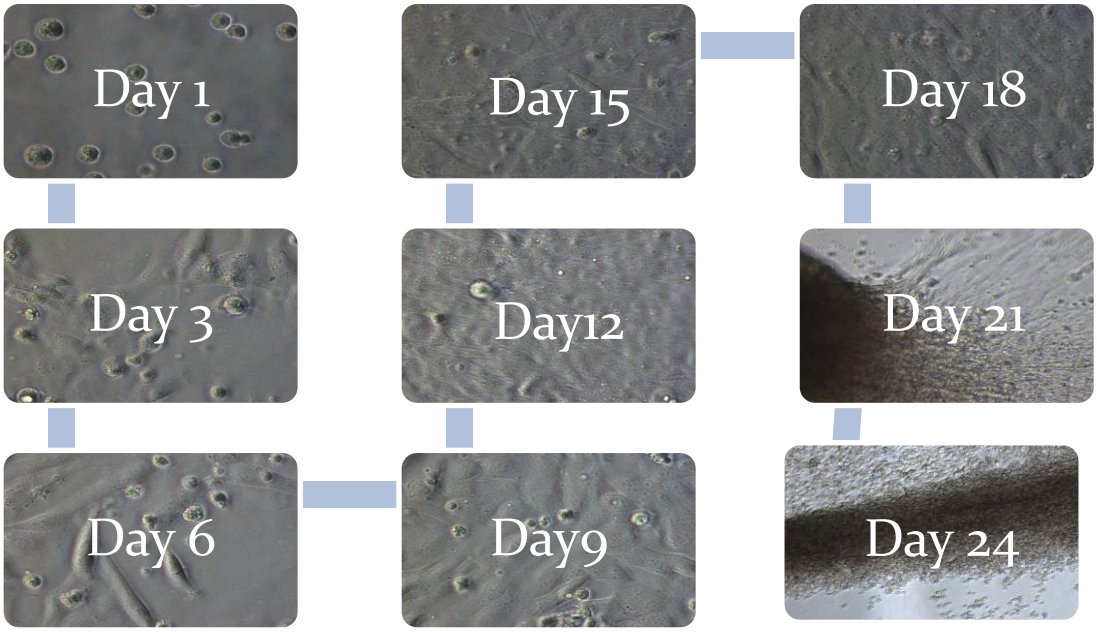

Figure 3.13: Images of hFob 1.19 cell in progress of growth for one month.

3.5.4 Cancerous human bone cell (U2OS)

Cancerous bone cell (U2OS) is from ATCC (Ponten et al., 1964). The base medium for this cell line is ATCC-formulated McCoy's 5a Medium Modified. The complete growth medium consists of the following components such as the base medium and 10% of fetal bovine serum added to a final concentration.

Cell culture starts with thawing of the frozen cell line. The thawed cell line will be transferred into the culturing flask for rejuvenation purpose. Cell medium will be change once every two days to maintain the nutrients needed for cells' growth. Bone cell is an adhesive cell type, therefore the cell will start to get attached to the bottom of the flask (day 6 in Figure 3.14). Due to the adhesive nature of the cell, liquid tripsin EDTA is used to detach the cell from the flask in order to subculture the cell line. Same procedure is applied in the process of collecting the cell from the flask for surface charge measurement. Cancerous bone cell line takes around 6 days to double in the amount of cell. Therefore, the subculture process is carried out every fortnight and cells are collected for surface charge measurement. The procedure for the culture is mentioned in section 3.5.2. The temperature for this cell line is maintained at 34^{o}C

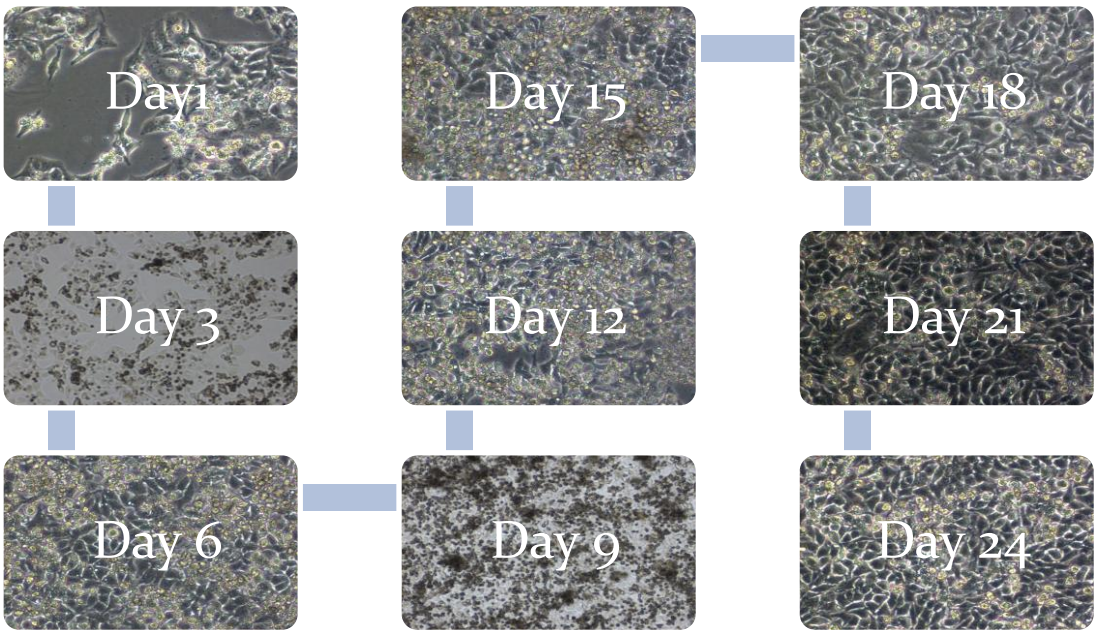

Figure 3.14: Images of U2OS cell in progress of growth for one month.

3.5.5 Cancerous human cervical cell (HeLa)

Cancerous human cervical cell line is from ATCC. The base medium for this cell line is ATCC-formulated Eagle's Minimum Essential Medium. The complete growth medium consists of the following components: fetal bovine serum to a final concentration of 10%.

Cell culture starts with the thawing of the frozen cell line. The thawed cell line will be transferred into the culturing flask for rejuvenation purposes. Cell medium will be change once every two days to maintain the nutrient needed for cell growth. Bone cell is an adhesive cell type, therefore the cell will start to get attached to the bottom of the flask (day 6 in Figure 3.15). Due to the adhesive nature of the cell, liquid tripsin EDTA is used to detach the cell from the flask in order to subculture the cell line. The same procedure is applied in the process of collecting the cell from the flask for surface charge measurement. Cancerous cervical cell line takes around 6 days to double in the amount of cell. Therefore, the subculture process is carried out every fortnight and cell is collected for surface charge measurement. The procedure for the culture is mentioned in section 3.5.2. The temperature for this cell line is 37^{o}C.

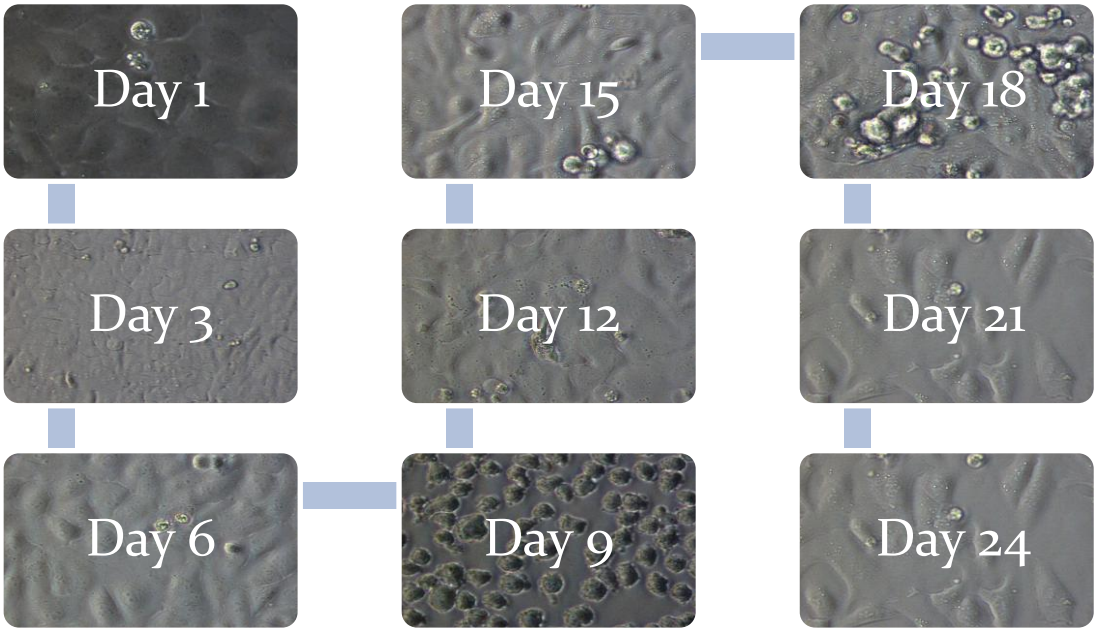

Figure 3.15: Images of HeLa cell in progress of growth for one month

The different growth rate of normal cells compared to cancerous cells has drawn our interest to study the causes. Some studies found that, biological cells are capable of communicating information between other cell and inside of the cell. These information play an important role is human body, which include regulation and integration of cell's growth. When cells become cancerous, these cells no longer maintain the natural function of the cells. Besides, cancerous cells also have their special feature that is totally varies from their normal counterpart. Healthy cells have a predictable growth rate, and form functional linkage between neighbouring cells and stop growing when they experiences injury and healing take place. Unlike normal cell, cancer cells are loosely attached and do not stop growing. These cancer cells do not possesses normal cell function, signalling and growth rate. In other word, cancer cell become independent from the rest of the body.

The growth results displayed in Figure 3.13 and Figure 3.14 show the different growth rate of the normal bone cell (hFob 1.19) and cancer bone cell (U2OS). The same growth medium Dulbecco's Modified Eagles's Medium (DMEM) is used for both cell culture. The growth of the cancerous bone cell is significantly faster than the normal bone cell. As shown in the image, the amount of cells after 6 days of culturing in normal bone cell remains the same amount. On the other hand, the cancerous bone cells showed a double amount of cells after merely 6 days of

culturing. The amount of normal bone cells is doubled in 12 days. The duration required for the normal bone cells to double up is twice as long compared to cancerous bone cells. At the same time, the growth of the normal bone cells population is decelerated during the 40th day of cell culture. While the cancerous bone cell population continue to grow in the process of cell culture.

3.6 Conclusion

In this study, surface charges of biological cell were measure by using the microelectrophoresis system. The image processing method was utilized in order to achieve the non invasive method for the surface charge measurement. This method had been carried out and result was reported in chapter 4. Image processing method also provides comprehensive information of the cell during the measurement. Surface charge of biological cell such as HeLa cell, U2OS and hFob 1.19 had been measured.

CHAPTER 4

RESULTS AND DISCUSSION

4.1 Introduction

In this section, the results of the suggested techniques for surface charge measurement (compact CCD microelectrophoresis) is presented. Surface charge of polystyrene bead is first measured using commercial instrument and the results are compared with the compact CCD microelectrophoresis. Polystyrene bead is also used for calibration of the CCD microscope; the calibrated image of polystyrene bead is displayed in this section. The surface charge of the biological cell is measured using the compact CCD microelectrophoresis system. Selected biological cells for this study includes yeast cells, normal bone cells (hFob 1.19), cancerous bone cells (U2OS) and cancerous cervical cells (HeLa). The results of the surface charge are presented and discussed in this section.

4.2 Surface Charge of Polystyrene Bead

4.2.1 Surface charge of polystyrene bead (10µm ± 0.1µm) using commercial product (Malvern instrument) microelectrophoresis

In this study, our microelectrophoresis system was calibrated for its magnification value and surface charge measurement with polystyrene beads. The calibration procedure was carried out by first capturing the image of the 10 µm size polystyrene

beads. The image of the beads is shown in Figure 4.2 where the polystyrene beads are spherical and consistently shaped. In general, the beads remain isolated from other beads contained in the solution; there was little aggregation of the polystyrene beads displayed in Figure 4.2. With the magnification of the modified webcam, 125 X, the measured EPM of this polystyrene bead is -1.17 μmcm/Vs in the DC electric field of 10V. Calibration process was performed before every set of data was acquired with the microelectrophoresis system. Using the calibration process, the focal length of the cell can be adjusted according to the height of the measurement chamber; images of beads floating in the middle of the chamber is captured and measured. This process is intended to avoid shear or drag force possession by the surface of the glass chamber which will affect the biological cell surface charge measurement. With the calibration process, the real time image capturing and EPM measurement system can deliver results with better consistency in uniform distinctive particles.

Surface charge of polystyrene bead is measured with the zitasizer commercial measurement instrument (Malvern instrument, UK) and our compact CCD microelectrophoresis system. The measured surface charge of the polystyrene bead using Malvern instrument is -1.32 $\mu mcm/Vs$ with the uncertainty of 5%. On the other hand, the measured surface charge value of the polystyrene bead using the compact CCD microelectrophoresis system is −1.17 μmcm$Vs/$ with an uncertainty of 10%. The variation of the result obtained by using the system of this study compared to commercial products is 13% (Figure 4.1). In one experiment, >> 20 unit of polystyrene beads were observed over the course of 10 seconds and the obtained data were computed to determine their direction of motion and velocity of beads. These spatial direction data, together with the applied electric field and velocity of the beads were used to compute the electrophoretic mobility of polystyrene beads. This outcome is obtained from the sample size of 100 polystyrene particles.

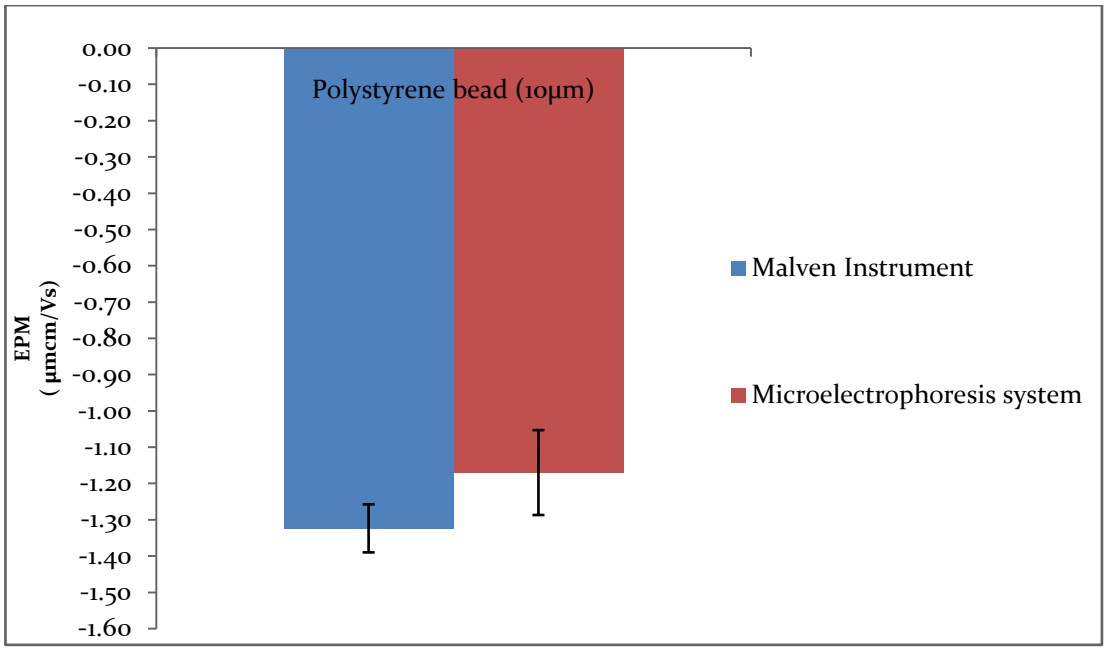

Figure 4.1: Surface charge of polystyrene bead using commercial instrument (Malvern instrument) and Microelectrophoresis system in this study.

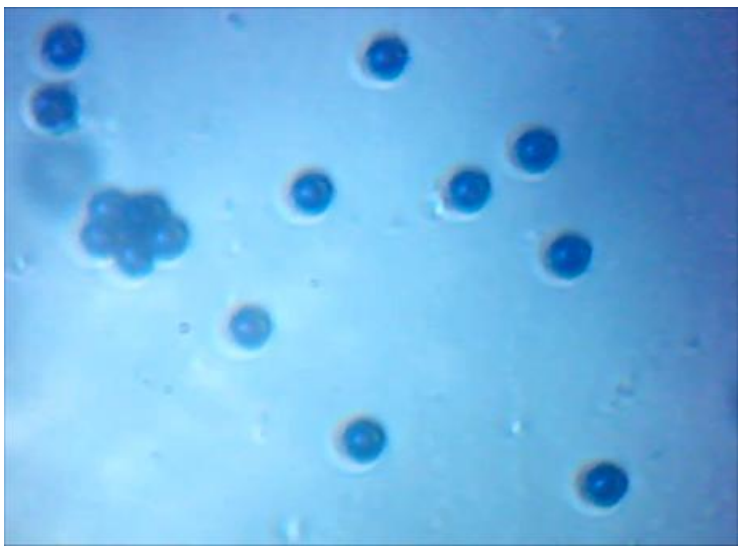

Figure 4.2: Image of polystyrene beads in two electrodes microelectrodephoresis system. The polystyrene beads are isolated from each other, only one aggregated group was found in the images captured.

4.3 Surface Charge of Yeast

4.3.1 Image of yeast captured with SEM and compact CCD microelectrophoresis system

Yeast as one of the selected biological cells in this study, provides an easily readied feed stock to be used to investigate the surface charge measurement. The image of yeast cells is first captured by using high magnification SEM. Figure 4.3 and Figure 4.4 show the yeast cell with magnification of 60 X, 900 X, and 5000 X. In Figure 4.3, the image of yeast cells with different magnification is presented. The image captured by SEM with 60 X magnification shows the group of yeast in a cylindrical form. These dried yeasts are closely packed together. With the magnification of 900 X, the yeast cells can be view clearly as the yeast is clumped together in dried form, but the individual cell size is hardly measured. Further magnification of 5000 X, the image in Figure 4.4 shows individual yeast cells, in which the size of the cells can be measured distinctively. In Figure 4.4, the average measured diameter of the yeast cell is 3.61 µm.

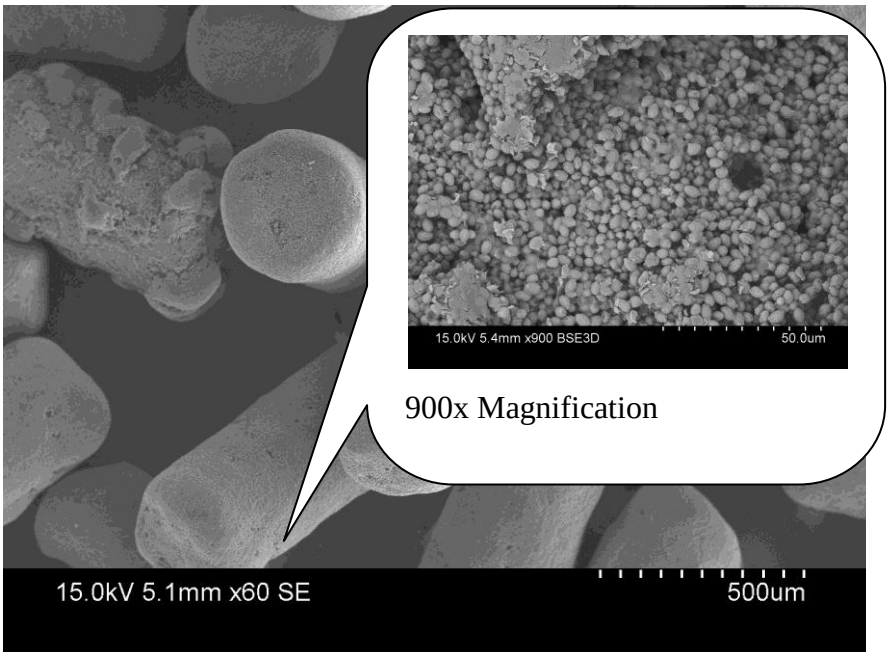

Figure 4.3: Yeast cell under SEM 60 X magnification, 900 x magnifications is displayed in the encrypted balloon. Yeast cell that appear in this process is dried and treated with gold coating procedure.

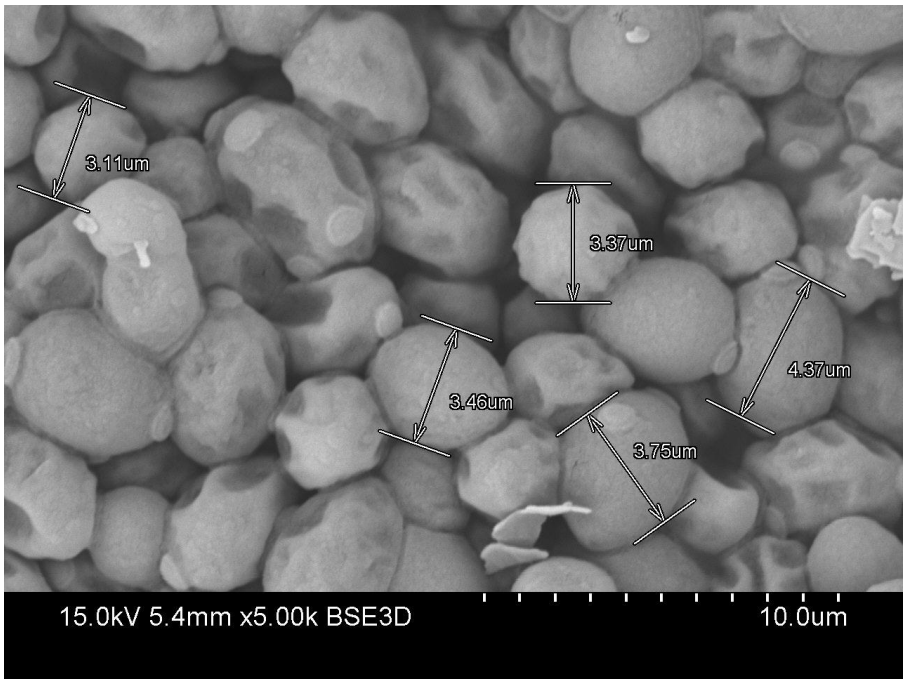

Figure 4.4: Yeast cell shown with SEM 5000 X magnification. The size of the yeast cell is observed clearly in the magnification level of 5000 X. The yeast cells are coated with gold before the SEM process.

On the other hand, in Figure 4.5, the image of yeast cells is captured using a compact CCD microscope microelectrophoresis system. The image is magnified 125 X and captured with the speed of 30 frames per second (fps). The compact CCD microscope microelectrophoresis system can obtain images of cell size ranging between 3µm to 15µm.The yeast cells in this image are measured with an average diameter size of 4 µm. This cost effective setting provides a clearer and more distinctive cell outline which is more suitable for the surface charge measurement of biological cells used in this study. In Figure 4.5, the yeast cells are isolated from each other and aggregations of the cell are rare. Therefore yeast cells are a suitable sample for biological cell surface charge measurement.

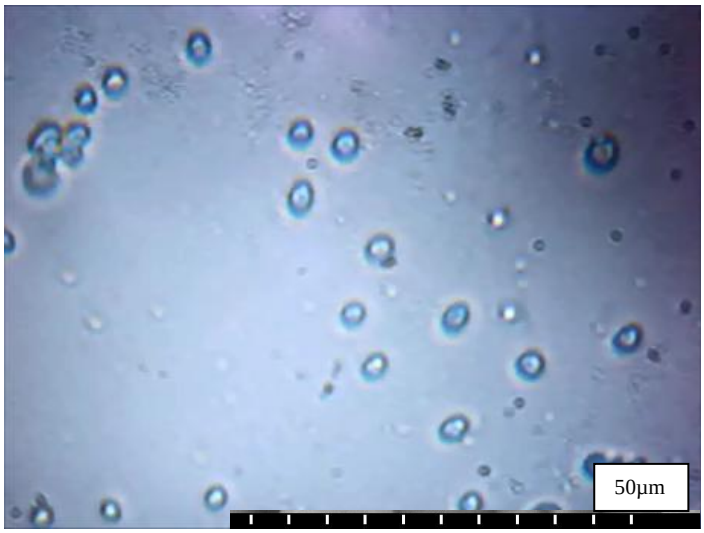

Figure 4.5: Image of Yeast cells with modified webcam in microelectrodephoresis system (125 X magnifications).

4.3.2 Surface charge measurement of yeast at pH range of 4.5 to 8.5 and applied voltage range from 5V to 25V

The surface charges of the yeast cells were measured with CCD microscope microelectrophoresis system. The measured surface charge as a function of pH is presented in Figure 4.6. The results show that the surface charge of the yeast is negatively charged in all the buffer solution (pH range 4 to 8). Results indicate the surface charge of the yeast ranges from -0.2 to -0.4 µmcm/Vs with a negative peak in pH 4.5 and pH 6.5. These two peaks may indicate yeast cell as a living cell react negatively to the buffer solution with pH 4.5 and pH 6.5. The yeast cell surface was surrounded with excessive negative ions at this pH level. Also mean that yeast cell may not be able to survive in this environment. At pH 6.5, the negativity of the surface charge is increased to -0.58 µmcm/Vs. This result demonstrates the similar trend reported by others although these authors used Malvern instrument zeta sizer 3000HS Advance for the measurement (Dobrzyn et al., 2013). The reported results showed the surface charge of the yeast is affected by the pH value of the buffer solution. Similarly, in this study, we found that the surface charge of the yeast is related to its suspended buffer's pH value.

With the same system and setup, the surface charges of yeast cells are measured in a changed of applied voltage, ranging from 5 V to 25 V which is shown in Figure 4.7. This investigation is to observe the changes of surface charge measurement due to the different electric field. The measured negative surface charges of yeast cells increases as the electric field increased. The maximum negative surface charge of yeast is recorded at the electric field of 25 V. The surface charge of yeast increases gradually from 5 V to 15 V. However, the yeast surface charge increase exponentially from 15 V to 25 V. In this study, applied voltage higher than 25 V would cause heat production and bubbles are formed at the electrodes which will affect the motion of the particles and calculation of the surface charge. When the voltage is too high, the Joule heating will cause the electrode to produce heat. The heat produced by the electrode will decrease the viscosity of the buffer solution where the mobility of the yeast cell increases. Therefore, voltages above 25 V will induce Joule heating which in turn, causes the mobility of the yeast cells to increase dramatically. This effect disables the surface charge measurement with the optical flow technique which limits the velocity to 15 pixel/second.

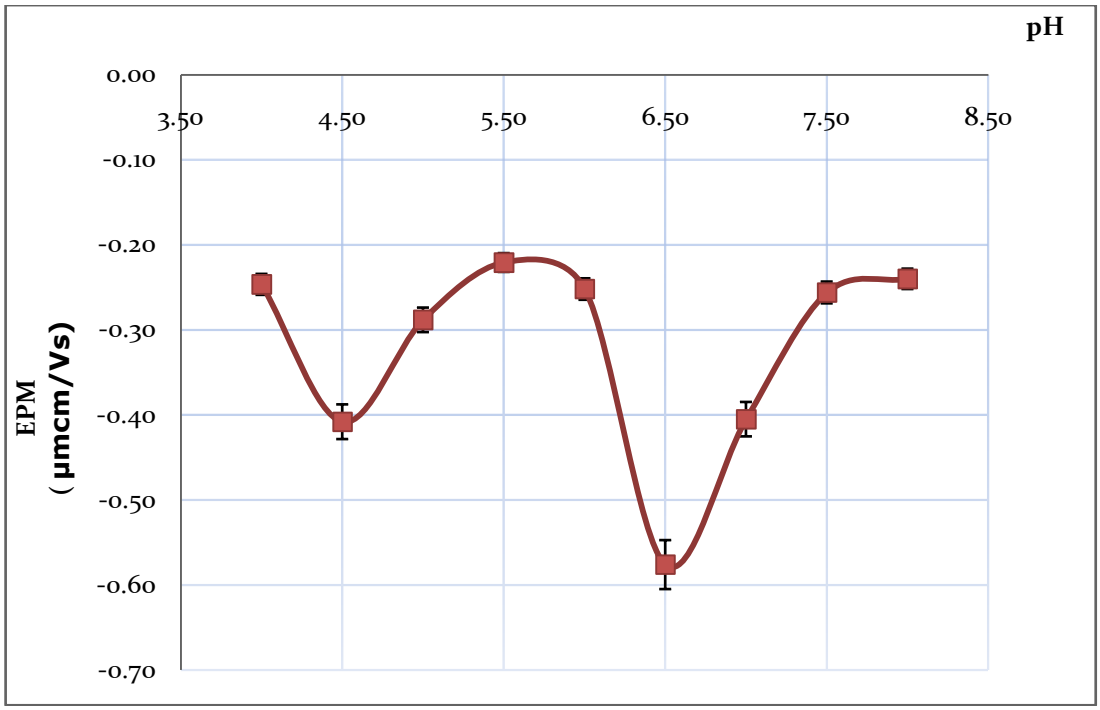

Figure 4.6: Surface charge of Yeast cell in two electrodes microelectrodephoresis system as a function of pH.

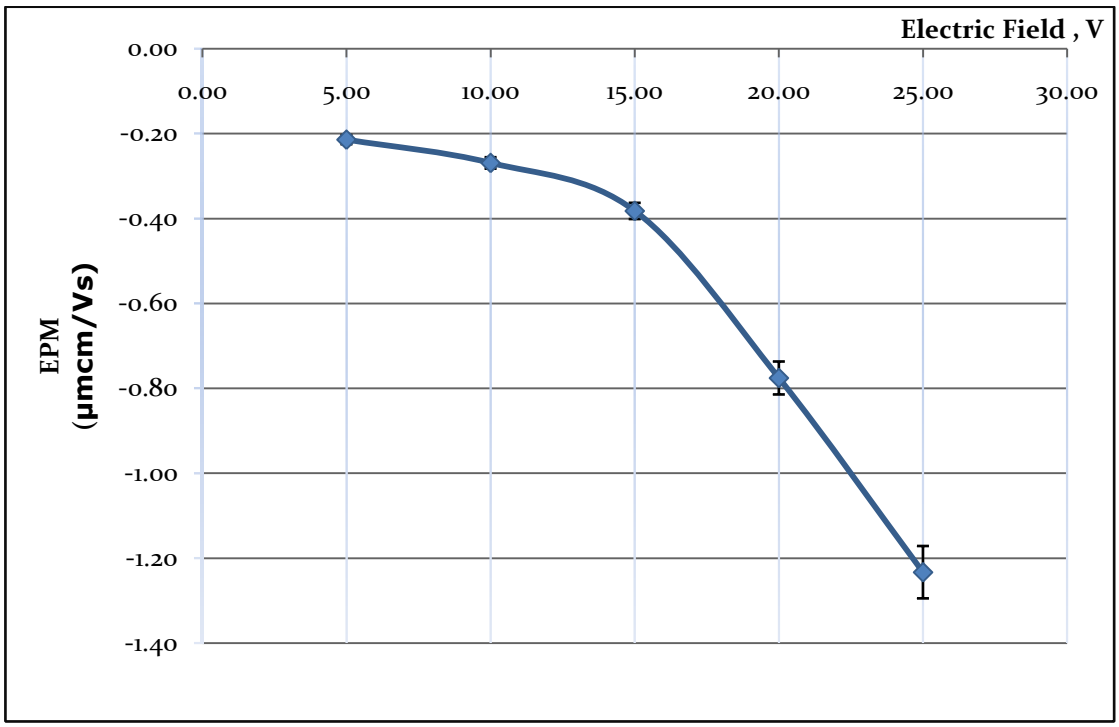

Figure 4.7: Surface charge of yeast in applied electric field of 5V to 25V (5V, 10V, 15V, 20V and 25V).

4.4 Surface Charge of Bone Cancer Cell (U2OS) and Bone Normal Cell (hFob 1.19)

Surface charge of normal bone cell (hFob 1.19) and cancerous bone cell (U2OS) are similarly shaped (Figure 4.8). The surface charge of the cells (normal and cancerous) is positive at pH value < pH 4.4. The isoelectrical point of the cell's surface charge is at the pH of 4.4. The results show that the surface charge of the bone cancer cells and normal bone cells used in this study is positive at pH 4 being 0.40 μmcm/Vs (cancer cell) and 0.54 μmcm/Vs (normal cell). From the results, indication of the surface charges of the cells is negatively charged as the pH value of buffer solution increase. Two different plateaus are presented in Figure 4.8. The first plateau is seen in between the pH value of 5 to 6 and the second form is in the pH value of 7 to 8. Both surface charges of bone cancer cells and normal bone cells shows similar patterns from pH 4 to pH 6. The obvious surface charge changed between both cells occurs at pH 6 till pH 8, in which the second plateaus of both cells have obviously departed from each other. This pH range is similar with the pH of human blood of pH 7.35 to pH 7.45. The surface charge of these two cells showed significant differences at the pH value near to human blood (Haven, 1941).

The surface charge of the cancer cells is highly negative in comparison to normal cells and this can be explained through the changes of cell membrane during tumorigenesis. The most crucial property of a cell membrane is its electrical charge and the potential difference in between the membrane and the surrounding solutions. Studies carried out by Dolowy had stated the cell membrane charges increase during the courses of tumorigenesis and decreases during necrosis (Dolowy, 1984). In normal cells, the anionic phospholipid are largely absent from the external leaflet of the plasma membrane under normal condition (Ran.S et al., 2002). Literature data shows that the exposure of the anionic phospholipids occurs during malignant transformation, cell injury, necrosis and apoptosis. Cancerous cell has an increase of the anionic phospholipids exposure which contributes to the highly negative charges of the cell in comparison to the normal cell.

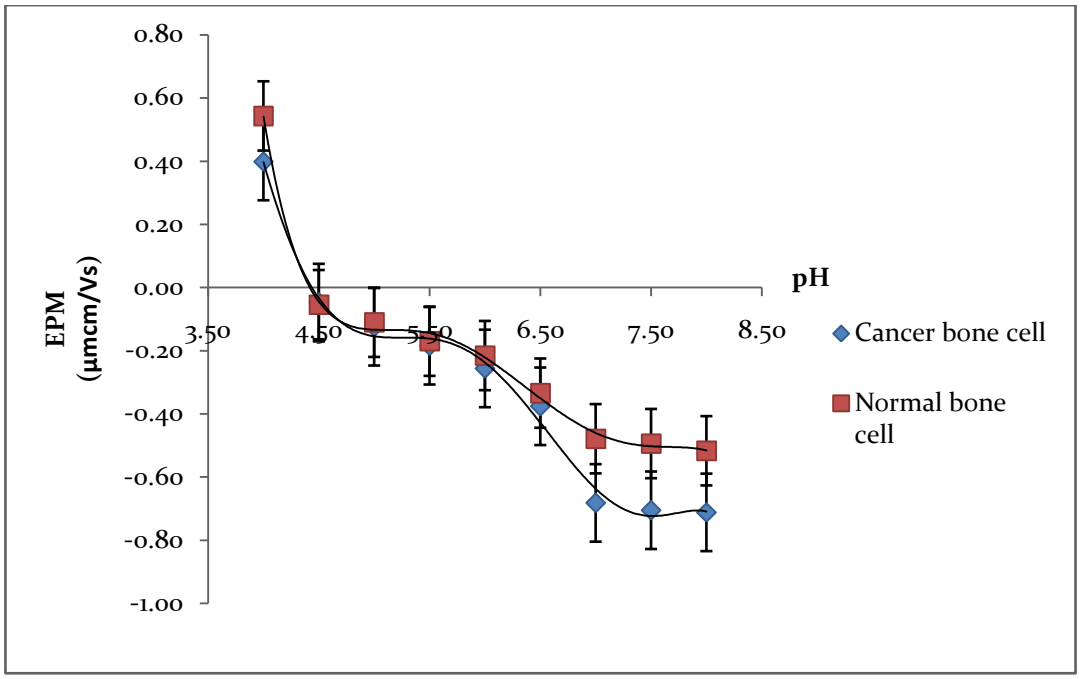

Figure 4.8: The surface charge of normal bone cell (hFob 1.19) and cancer bone cell (U2OS) as a function of surface charge in different buffer solution.

4.5 Surface Charge of Cervical Cancer Cell (HeLa)

The surface charge of the HeLa cell as a function of pH is presented in Figure 4.9. The surface charge of HeLa cells is positive at pH 4.5 with the surface charge value of 0.64 µmcm/Vs. The surface charge of the HeLa cells reaches isoelectric point at pH 4.8. As the pH increases, the measured surface charge of the HeLa cell is negatively charged. It can be seen in the Figure 4.9, where the surface charge of HeLa cells and U2OS in the function of pH is similar in shape. Although both surface charge results shows a similar trend, yet the surface charge of HeLa cancer cell is higher than the U2OS at pH value of pH 5 to pH 6.5 as displayed in Figure 4. 9. These phenomena occur due to the different surface area of the cell. As scientist had found that the membrane's lipid bilayer mutated during the cancer transformation (Szachowicz-Petelska et al., 2012). At pH 7 and above, surface charge of U2OS is higher than the HeLa cell. Both results also displayed two layers of plateau as mentioned in section 4.4.

Scientists repeatedly presented that modification of the membrane's lipid bilayer occur during cancer transformation (Szachowicz-Petelska et al., 2012; Punnonen et al., 1989). Studies had suggested that the phospholipids content of human breast cancer cells increases in comparison to the normal counterparts (Podo et al., 2007; Sakai, 1992; Punnonen et al., 1989). Cancer cell replicate rapidly in comparison to the normal cell hence increased in phospholipids content encourage the cell membrane synthesis which is closely related to the fast replication process (Ruiz-Cabello et al., 1992). Increased amounts of phospholipids on the membrane causes higher amount of functional groups: phosphate group, amino acid group, and carboxy group. While in acidic buffer medium (low pH), the charge of the membrane are due to the amino groups, whereas in basic buffer solution with high pH value, it is greatly due to the carboxyl and phosphate group. Surface charge of these cells are closely related to the amount of phospholipids on the membranes, where cells are found to be negatively charged in high pH values while positively charged at low pH values. Hence, increased phospholipids in cancer cell can cause the surface charge of the cell to increase negatively in high pH buffer medium.

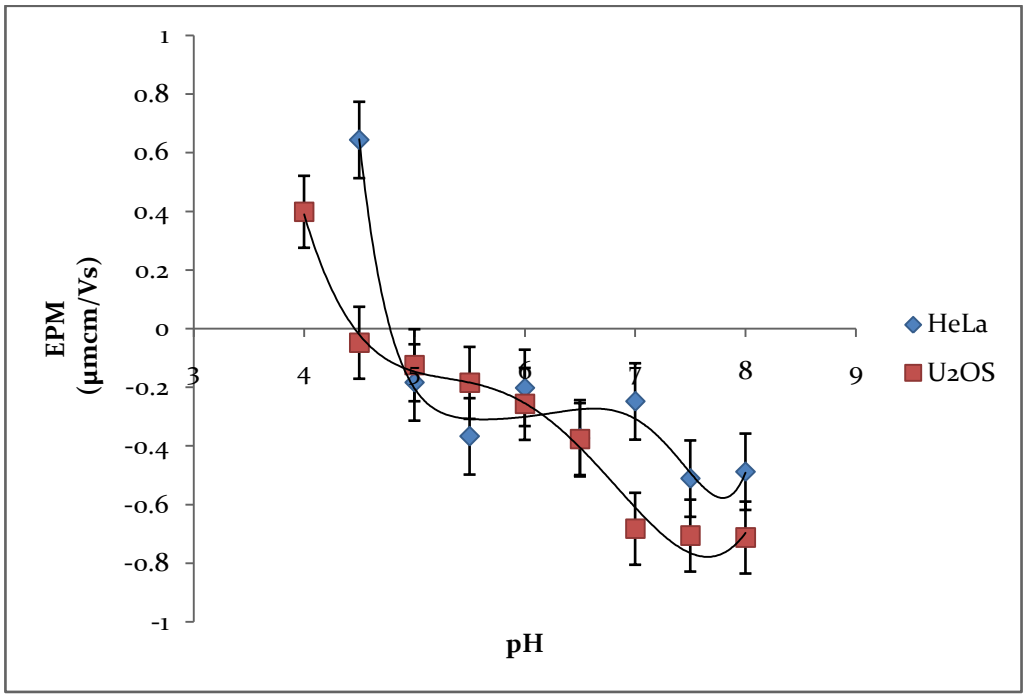

Figure 4.9: Comparison between Surface charge of cervical cancer cell (HeLa) and Bone cancer cell (U2OS) in different pH.

CHAPTER 5

CONCLUSION AND RECOMMENDATIONS

5.1 Conclusion

In this study, the compact CCD microscope was built and designed with microelectrophoresis method to measure the surface charge of biological cells. The designed compact microscope is able to capture images of cells with the magnification power of 125x. The captured images are then sent to image processing for image acquisition and surface charge measurement. This process is accomplished in an automated manner with MatLab program. Results of the cells' surface charge is displayed together with the original image captured using our system. The automated system allows the measurement of cell's surface charge with image of cells or particle being measured.

At the same time, the surface charge of yeast cells, normal bone cells (hFob 1.19), cancerous bone cells (U2OS), and cancerous cervical cells (HeLa) is measured using the compact CCD microelectrophoresis system with optical flow method. This image processing method has successfully measured the surface charge of the biological cells selected in this study. Measurement of cells' surface charge in the applied electric field is limited to one layer of cells at a time. Measured surface charges are in an average value of the first 20 to 50 cells that had pass through the field of view of the imaging system. The results show a significant pattern in between surface charge of normal bone cells (hFob 1.19) and cancerous bone cells (U2OS). Surface charge of cancer cells is highly negative in comparison to normal

cells at pH values close to human blood (pH 7.35 to pH 7.45). This finding shows a promising reason for cancer diagnostic using blood serum in the future.

The designed compact CCD microelectrophoresis system with image processing has demonstrated and proven that it is suitable for automated surface charge measurement of biological cells with size range from 4 to 20 µm. In addition, we have built the system successfully with cost effective materials.

5.2 Recommendation

Studies of cell's surface charge have shown results in differentiating the normal cell and diseased cells such as cancer cells. Measured surface charge value can be used for early detection or diagnosis of cell's health status. We propose to improve the system with the 'lab on chip (LOC)' technology. The LOC method can minimize the measurement chamber and provide a sterile condition from the culturing of cell to surface charge measurement. Furthermore, LOC materials provide a clearer view for measurement of surface charge. Images of the measurement chamber can be acquired through the transparent material of the LOC measurement chamber.

At the same time, the imaging system will be upgraded in the function of auto focus of field of view. The auto focus function will assist in measuring the surface charge of cells in different layers within the measurement chamber. This will allow more cells to be captured in the same layer and measurement is done with higher repetition taken in one sample. Auto focus function will be performed by using the Ultrasonic motor powered auto focus lens. This lens will enable the lens to shift according to the targeted focus point. An additional benefit of the autofocus function is that the surface charge measurement can be performed without any manual adjustment of the focus point.

In future, the sample of the experiment may include red blood cells of dengue fever patients. Measuring the surface charge of the red blood cells will be compared with the normal healthy person. The difference in surface charge could be the key for early detection of the deadly disease that has become pandemic in Malaysia. Other

deadly disease may be detected by using the measured surface charge of the red blood cell.

REFERENCES

Allison, S. 2007 Liposomal Drug Delivery. *Journal of Infusion Nursing* , 30 (2),pp.89–95

An, J., Lee, J., Lee, S., Park, J., and Kim, B., 2009. Separation of malignant human breast cancer epithelial cells from healthy epithelial cells using an advanced dielectrophoresis-activated cell sorter (DACS). *Analytical and Bioanalytical Chemistry,*. 394 (3), pp.801-809.

Barz, D. P. J. and Ehrhard, P., 2005. Model and verification of electrokinetic flow and transport in a micro-electrophoresis device. *Colloids and Surfaces,*5 (9), pp. 949–958.

Camp, J. P., and Capitano, A. T., 2005. Size-dependent mobile surface charge model of cell electrophoresis. . *Colloids and Surfaces,* 113, pp. 115–122.

Chaprenet, J., Berton-carabin, C. C., Elias, R. J., and Coupland, J. N., 2014. Food Hydrocolloids Effect of interfacial properties on the reactivity of a lipophilic ingredient in multilayered emulsions. *Food Hydrocolloids*, 42, pp. 56–65.

Chen,Y., Ladi, E., Herzmark, P., Robey, E. and Roysam, B., 2009. Automated Danalysis of cell migration and interaction in the thymic cortex from time-lapse sequences of 3-D multi-channel multi-photon images. *Journal of Immunological Methods,* 340, pp. 65–80.

Corbett, J.C.W. et al., 2012. Measuring surface zeta potential using phase analysis light scattering in a simple dip cell arrangement. *Colloids and Surfaces A: Physicochemical and Engineering Aspects,* 396, pp.169–176.

Coulter, B. Y. C. B. and Fellow, V. C., 1920. The isoelectric point of red blood cells and its relation to agglutination. *The Journal of General Physiology*, 3 (3), pp. 309-323.

Debeir, O., Ham, P.V., Kiss, R. and Decaestecker, C., 2005. Tracking of migrating cells under phase-contrast video microscopy with combined mean-shift processes. *IEEE Transactions on Medical Imaging,* 24, pp. 697–711.

Dextras, P., Burg, T.P. and Manalis, S.R., 2009. Integrated Measurement of the Mass and Surface Charge of Discrete Microparticles Using a Suspended Microchannel Resonator. *NIH*, 81 (11), pp.4517–4523.

Dobrzyn, I., and Figaszewski, Z. A., 2013. Changes in Electric Properties of Human Breast Cancer Cells, *Biomedical Microdevices,* 10, pp. 161–166.

Dolowy, K.,1984. Bioelectrochemistry of cell surface. *Progr. Surface Sci.,* 15, pp. 245-368

Dormann, D. and Weijer, C.J., 2006. Imaging of cell migration. , *Biomedical Microdevices*, 25 (15), pp.3480–3493.

Gascoyne, P.R.C., Noshari, J., Becker, F.F., and Pethig, R., 1994. Use of dielectrophoretic collection spectra for characterizing differences between normal and cancerous cells., *IEEE Transactions on industry Applications,* 30 (4), pp. 829-834.

Harris, S.A. and Spelsberg, T.C., 1997. Immortalized human fetal osteoblastic cells. *US Patent* 5,681,701

Hashimoto, N. et al., 1998. Cell electrophoretic mobility and glycerol lysis of human erythrocytes in various diceases. *Electro phoresis,*19, pp 1227–1230.

Hunter., R. J., 1981. *Zeta Potential in Colloid Science: Principles and Applications*, London: Academic Press.

Howe, A. M., 2000. Some aspects of colloids in photography. *Current Opinion in Colloid & Interface Science, 5* (5-6), pp. 288–300

Jitendra, N. and Mehrishi, J. B., 2002. Electrophoresis of cells and the biological relevance of surface charge. *Electrophoresis, 23* (13), pp. 1984–1994.

Karner, S., and Anne, N., 2011. The impact of electrostatic charge in pharmaceutical powders with specific focus on inhalation-powders. *Journal of Aerosol Science, 42* (6), pp.428–445.

Kachouie, N.N., Fieguth, P., Ramunas, J. and Jervis, E., 2006. Probabilistic model-based cell tracking. *International Journal of Biomedical Imaging*, pp. 1–10

Kaysinger, K. K., and Ramp, W. K., 1998. Extracellular pH modulates the activity of cultured human osteoblasts. *J. Cell. Biochem.,* 68 (1), pp. 83-89.

Kremser, L., Blaas, D. and Kenndler, E., 2004. Capillary electrophoresis of biological particles: viruses, bacteria, and eukaryotic cells. *Electrophoresis,* 25 (14), pp. 2282–91.

Labarca, P., and R. Lattore ., 1992. Insertion of ion channels into planar lipid bilayers by vesicle fusion. *In Methods in Enzymology*, 207, pp. 447–463.

Lopez-Garcia, J.J, Horno, J., Gonzalez-Caballero, F., Grosse, C. and Delgado, A. V., 2000. Dynamics of the electric double layer: Analysis in the frequency and time domains. *Journal of Colloid and Interface Scien*ce, 228(1).

Poo, M., Lam, J.W., Orida, N. and Chao, A.W. 1979., Electrophoresis and diffusion in the plane of cell membrane. *Biophysical journal*, 26 (1), pp. 1–22.

Lin, G. et al., 2007. A multi-model approach to simultaneous segmentation and classification of heterogeneous populations of cell nuclei in 3D confocal microscope images. *Cytometry Part A*, 71, pp. 724–36.

Latorre, R., Labarca, P. and Naranjo, D., 1992. Surface charge effects on ion conduction in ion channels. *Methods Enzymol*,207: pp. 471-501.

Masliyah., J. H., 1994. Electrokinetic transport phenomena, *The alberta oil sands technology and research authority technical publication*, series 12, Canada: Edmonton.

Mehrishi., J. N. and Bauer, J., 2002. Review Electrophoresis of cells and the biological relevance of surface charge. *Electrophoresis* , 23 (13), pp.1984–1994.

Meijering, E., Dzyubachyk, o., smal, I., Van cappellen, W. A., 2009. Tracking in cell and developmental biology. *Seminars in Cell & Developmental Biology* , 20 (8), pp.894–902.

Peng, W. P. et al., 2008. Charge Monitoring Cell Mass Spectrometry. *Analytical Chemistry*, 80 (7), pp.2524–2530.

Piasecki, W., Salwirski, L. and Froncisz, W., 1997. New Model of Charged Molecule Redistribution Induced in Spherical Vesicles by Direct Current Electric Field. *Biophysical Journal*, 72, pp.613–618.

Podo. F. et al., 2007. Abnormal choline phospholipid metabolism in breast and ovary cancer: molecular bases for noninvasive maging approaches. *Current Medical Imaging Review*, 3, pp.123–137

Ponten, J. and Saksela, E., 1967. Two established in vitro cell lines from human mesenchymal tumours. *International Journal of Cancer*, 2 (5), pp. 434-447.

Probstein., R. F., 1994. *Physicochemical Hydrodynamics: Introduction* , 2nd ed. New Jersey: John Wiley & Sons.

Punnonen, K., Hietanen, E., Auvinen, O. and Punnonen, R., 1989. Phospho-lipids and fatty acid in breast cancer tissue. *Journal of Cancer Research Clinical Oncology* , 115, pp. 575–578

Ran, S., Downes, A. and Thorpe, P.E., 2002. Increased exposure of anion phospholipids on the surface of tumor blood vessels. *Cancer Res* , 62, pp. 6132–6140

Ruiz-Cabello, J., and Cohen, J.S., 1992. Phospholipids metabolites as indicators of cancer cell function. *NMR Biomedical* , 5, pp. 226–233.

Sakai, K., 1992. Composition and turnover of phospholipids and neutral lipids in human breast cancer and reference tissues. *Carcino-genesis* ,13 (4), pp.579–584

Simionescu, M. Antohe, F. and Heltianu, C., 1991. Albumin-binding proteins of endothelial cells: immunocyto chemical detection of the 18 kDa peptide. *European Journal of cell Biology*, 56, pp. 34-42.

Seaman, G. V. F., 1965. Electrophoresis using a cylindrical chamber. In: *Ambrose, E. J. (Ed.). Cell electrophoresis*, pp. 4–21.

Slivinsky, G. G., Hymer, W. C., Bauer, J. and Morrison, D. R., 1997. Cellular electrophoretic mobility data: a first approach to a database. *Electrophoresis,*18 (7), pp.1109–1119.

Smoluchowski, M. Z., 1917. Versuch einer mathematischen theorie der koagulation skinetik kolloider losugen. *Physic Chemistry*, 92, pp.129-168.

Szachowicz, P. B., Dobrzynzeit, I., Sulkowski, S., Figaszewski, Z.A., 2012 Characterization of the cell membrane during cancer transformation. *Journal of Environment biology*, 31 (5), pp. 845–850.

Ta, V., Lezoray, O., Elmoataz, A., and Schupp, S., 2009. Graph-based tools for microscopic cellular image segmentation. *Pattern Recognition*, 42 (6), pp.1113–1125.

Takahashi, N. et al., 2011. Proposal and experimental validation of the electrophoretic Coulter method for analyzing microparticles and biological cells. *Sensors and Actuators B: Chemical*, 151 (2), pp.410–415.

WHO, 2014. *The top 10 causes of death Fact sheet N°310* [Online]. Available at: http://www.who.int/mediacentre/factsheets/fs310/en/ [Accessed: 8th August 2014].

VanOss, C.J., 1994. Interfacial Forces in Aqueous Medium. Florida: CRC press.

Wählby, C., Sintorn, I.M., Erlandsson, F., Borgefors. G. and Bengtsson, E., 2004. Combin-ing intensity, edge and shape information for 2D and 3D segmentation of cell nuclei in tissue sections. *Journal of Microscopy*, 215, pp. 67–76.

Yang, X., Li, H. and Zhou, X., 2006. Nuclei segmentation using marker-controlled watershed, tracking using mean-shift, and Kalman filter in time-lapse microscopy. *Circuits and Systems I: Regular Papers, IEEE Transactions on*, 53 (11), pp. 2405–14.

Zhang, Y., Yang, M., Park, J., Singelyn, J., and Sailor, M. J., 2011. NIH Public Access, *5* (17), pp. 1990–1996.

Zhou, X., Li, F., Yan, J., and Wong, S.T.C., 2009. A novel cell segmentation method and cellphase identification using Markov model. *Information Technology in Biomedicine, IEEE Transactions on*,13 (2), pp.152–157.

APPENDICES

APPENDIX A Publication

Publication available online :

Teoh B. Y., Y. T. Khok, P. F. Lee The Simple Setting of Microfluidic System with Microelectrophoresis Setup for Surface Charge Measurement. *The 15th International Conference on Biomedical Engineering IFMBE Proceedings Volume 43, 2014, pp 838-841*doi 10.1007/978-3-319-02913-9_216

Teoh, B.Y.; Fong, Y.S.; Lee, P.F., "Compact surface charge diagnostic device," *Biomedical Engineering (ICoBE), 2012 International Conference on* , vol., no., pp.490,493, 27-28 Feb. 2012 doi: 10.1109/ICoBE.2012.6179065

Pending publication:

IET Circuits, Devices & Systems:

Teoh B. Y., P. F. Lee, Y. H. Tay, T. K. Yong,. Real-time Surface Charge Measurement of Discrete Microparticle Using Micro Electrophoresis and Compact CCD Microscope. ID: CDS-2014-0392.

Journal of Biomedical Science :

Teoh B. Y. and Lee, P. F., Surface Charge of Biological Cell Using Micro Electrophoresis and Compact CCD Microscope

Winning award:

BES-SEC Students' Design Competition in National University of Singapore 2013, Merit award (Top 6th project) was awarded to our project out of 30 over projects participated from around the world. The certification is displayed in Figure 5.1.

Figure 5.1: Certification of Merit award from BES-SEC students' Design competition in NUS Singapore.

APPENDIX B: Computer Programme Listing

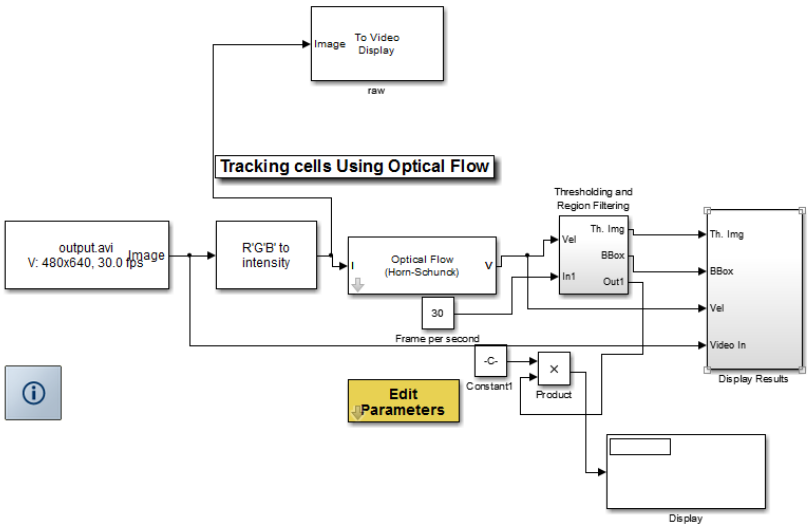

Figure 5.2: Overall design of the image processing program using MatLab.

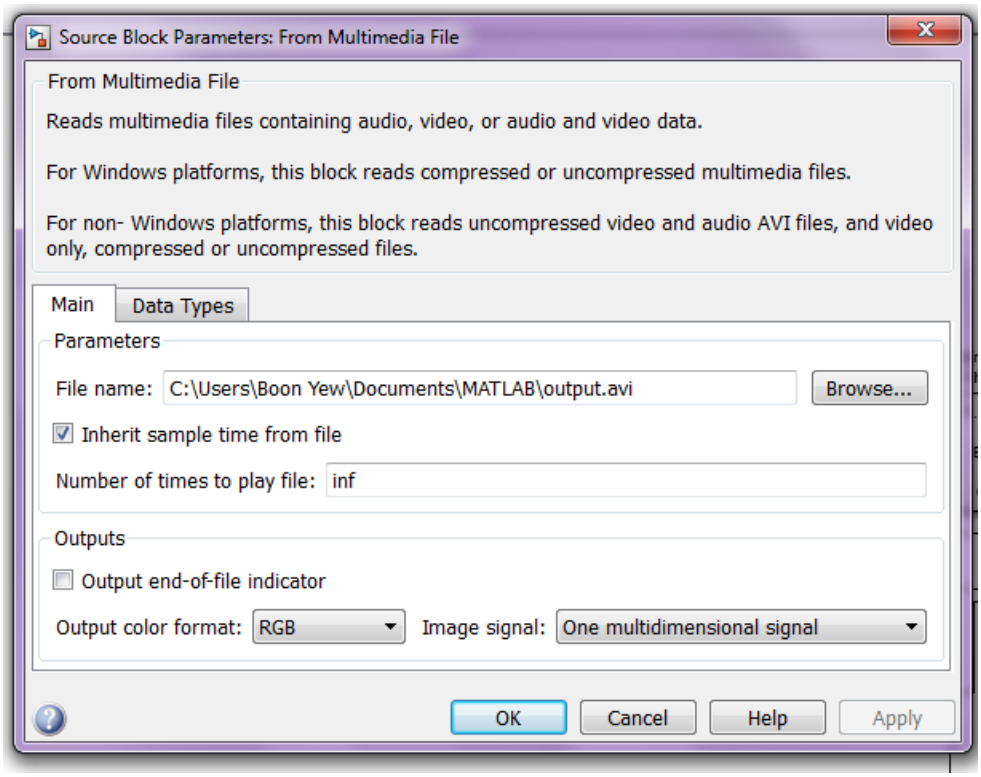

Figure 5.3: Setting of the image acquisition block, where it obtain RGB images.

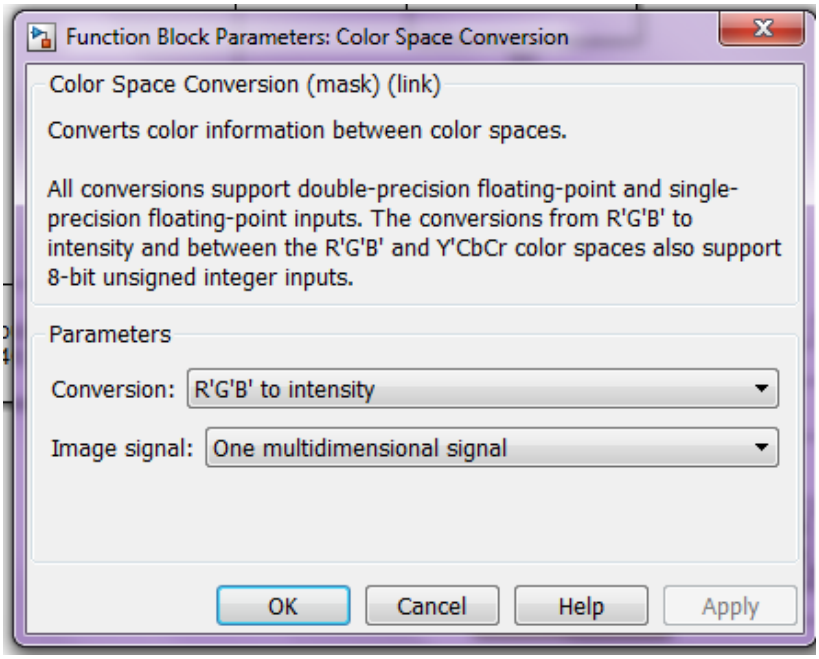

Figure 5.4: Setting of the image conversion block, where the image data is convert from RGB to intensity

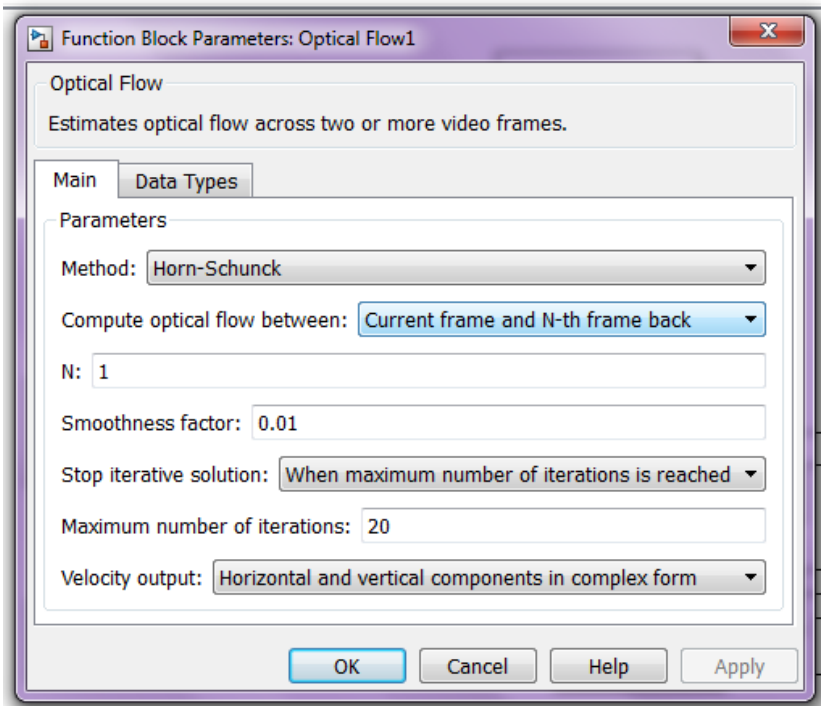

Figure 5.5: Setting of the horn-schunk image processing block, where all the parameter was set and mentined in section 3.

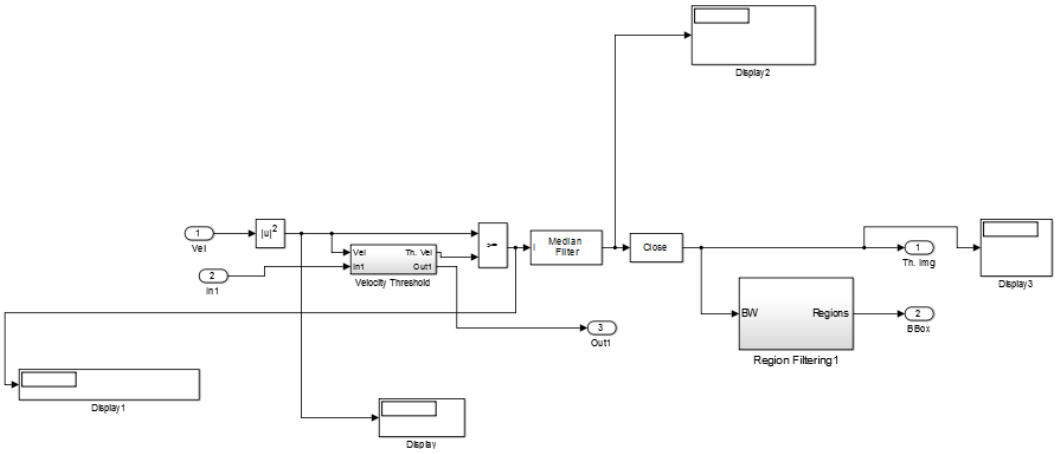

Figure 5.6: Sub block program to filter the interested region from back ground noise. The region of the interest are sent to the sub block for mean velocity calculation.

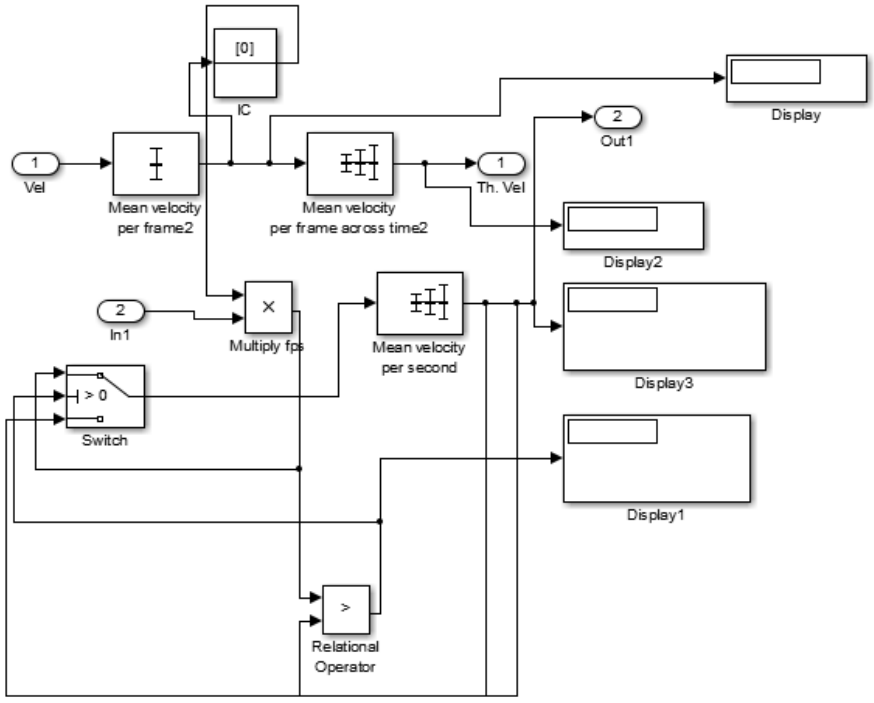

Figure 5.7: Sub block build to determine the threshold velocity for filtering and determine the electrophoretic mobility (EPM).

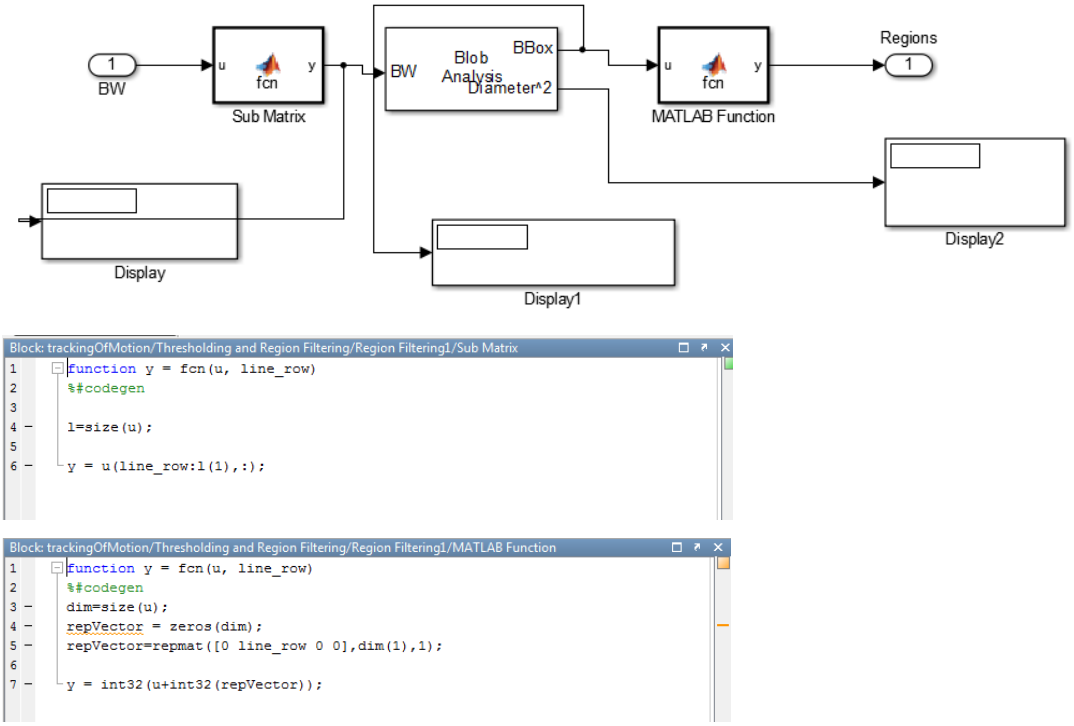

Figure 5.8: Sub block build to determine the size of the targeted cell and pass to sub block for drawing of boundary.

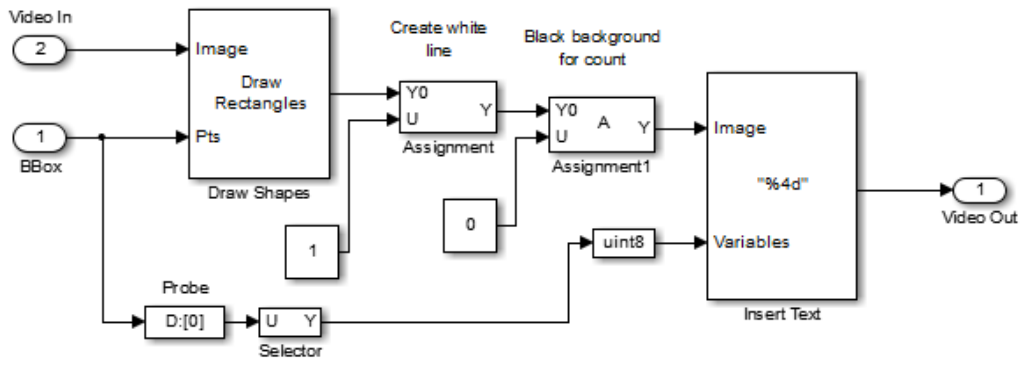

Figure 5.9: Sub block build to draw the boundary of the cell with green box.

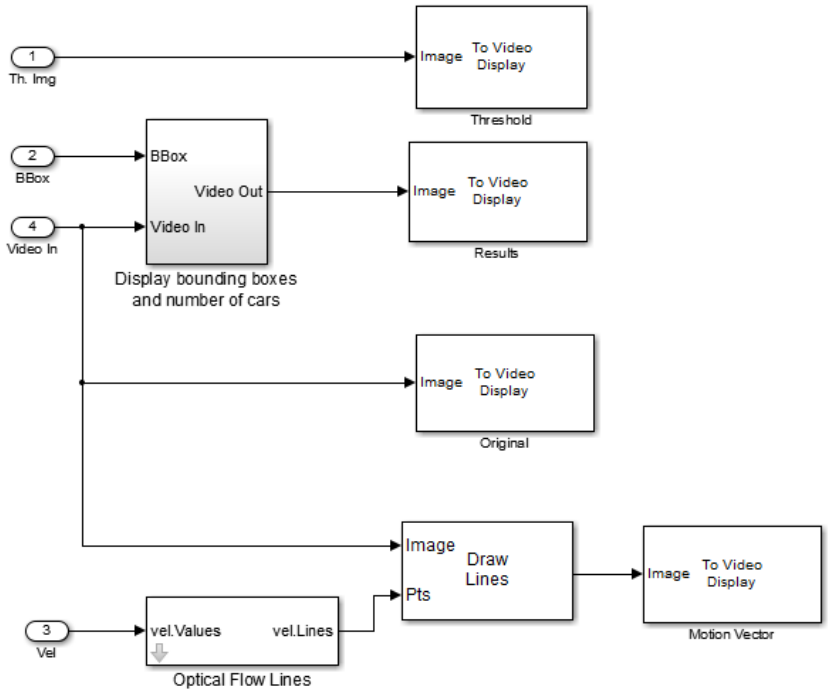

Figure 5.10: Sub block build to display the desired result, such as the raw image of the cell, image of cell with results (green box), image of cell with motion vector showing the direction of movement.